

## $\beta$ Decay and Isomeric Properties of Neutron-Rich Ca and Sc Isotopes

H. L. Crawford<sup>1,2</sup>, R. V. F. Janssens<sup>3</sup>, P. F. Mantica<sup>1,2</sup>, J. S. Berryman<sup>1,2</sup>,  
 R. Broda<sup>4</sup>, M. P. Carpenter<sup>3</sup>, N. Cieplicka<sup>4</sup>, B. Fornal<sup>4</sup>, G. F. Grinyer<sup>2</sup>, N. Hoteling<sup>3,5</sup>,  
 B. P. Kay<sup>3</sup>, T. Lauritsen<sup>3</sup>, K. Minamisono<sup>2</sup>, I. Stefanescu<sup>3,5</sup>, J. B. Stoker<sup>1,2</sup>,  
 W. B. Walters<sup>5</sup>, and S. Zhu<sup>3</sup>

<sup>(1)</sup> Department of Chemistry, Michigan State University, East Lansing, Michigan 48824

<sup>(2)</sup> National Superconducting Cyclotron Laboratory,

Michigan State University, East Lansing, Michigan 48824

<sup>(3)</sup> Physics Division, Argonne National Laboratory Argonne, Illinois 60439

<sup>(4)</sup> Institute of Nuclear Physics, Polish Academy of Sciences Cracow, Poland PL-31342 and

<sup>(5)</sup> Department of Chemistry and Biochemistry, University of Maryland, College Park, Maryland 20742

(Dated: July 2, 2010)

The isomeric and  $\beta$ -decay properties of neutron-rich  $^{53-57}\text{Sc}$  and  $^{53,54}\text{Ca}$  nuclei near neutron number  $N=32$  are reported, and the low-energy level schemes of  $^{53,54,56}\text{Sc}$  and  $^{53-57}\text{Ti}$  are presented. The low-energy level structures of the  $_{21}\text{Sc}$  isotopes are discussed in terms of the coupling of the valence  $1f_{7/2}$  proton to states in the corresponding  $_{20}\text{Ca}$  cores. Implications with respect to the robustness of the  $N=32$  subshell closure are discussed, as well as the repercussions for a possible  $N=34$  subshell closure.

PACS numbers: 23.40.-s, 23.20.Lv, 21.10.Hw, 29.38.Db, 27.40.+z

Keywords:  $^{53-57}\text{Sc}$

### I. INTRODUCTION

The nuclear shell model [1] was developed in part to explain the observed extra stability of nuclei along the valley of  $\beta$  stability corresponding to ‘magic’ numbers of protons and/or neutrons. The magic numbers at 2, 8, 20, etc. were explained as corresponding to closed-shell nucleonic configurations. While the shell model is robust near stability, there is evidence at the extremes of the nuclear chart that the single-particle level ordering changes, leading to the erosion of some shell closures and/or the appearance of new ‘magic’ numbers in exotic nuclei. The attractive proton-neutron monopole interaction [2] can produce drastic changes in level ordering, and in regions of low single-particle density, result in modified shell gaps. For example, the monopole shift of the  $\nu 1f_{5/2}$  orbit with changing  $\pi 1f_{7/2}$  occupancy has been invoked to explain the observed  $N=32$  subshell closure in nuclei in the neighborhood of the doubly-magic nucleus  $^{48}_{20}\text{Ca}$ .

The  $N=32$  subshell closure has been well-established experimentally in  $_{20}\text{Ca}$  [3, 4],  $_{22}\text{Ti}$  [5] and  $_{24}\text{Cr}$  [6] on the basis of the systematic behavior of the  $E(2_1^+)$  energies as a function of neutron number in the even-even nuclei of these isotopic chains. Additional evidence for  $N=32$  as a new subshell closure in neutron-rich nuclei below  $Z=28$  comes from the low  $B(E2 : 2^+ \rightarrow 0^+)$  transition probabilities measured for  $^{54}\text{Ti}$  [7] and  $^{56}\text{Cr}$  [8]. The high-spin structures of  $^{50,52,54}\text{Ti}$  [5] are also indicative of a sizeable  $N=32$  shell gap. The separation between the  $6_1^+$  and the closely spaced  $8_1^+, 9_1^+$  and  $10_1^+$  levels in  $^{54}\text{Ti}$  was taken to indicate the substantial energy cost in promoting a  $2p_{3/2}$  neutron to either of the  $\nu 2p_{1/2}$  or  $\nu 1f_{5/2}$  orbitals.

Migration of the  $\nu 1f_{5/2}$  orbit may be such that, beyond  $N=32$ , a gap between the  $\nu 2p_{1/2}$  and the  $\nu 1f_{5/2}$  orbitals

develops. The results of shell-model calculations with the GXPF1 effective interaction point to a  $N=34$  subshell closure in the neutron-rich Ti and Ca isotopes [9]. The prediction of a new magic number at  $N=34$  for the Ti isotopes is inconsistent with experimental results in  $^{56}\text{Ti}$  [7, 10]. However, shell-model calculations with the slightly-modified GXPF1A effective interaction [11] suggest that a  $N=34$  subshell gap may still be present in the Ca isotopes.

While the level structure of  $^{54}\text{Ca}$  remains difficult to reach experimentally, the possible development of a  $N=34$  shell closure in this region can be examined indirectly. Some insight into the relative collectivity of the  $_{20}\text{Ca}$  isotopes can be obtained from the energy separation between the  $(\pi 1f_{7/2})_{7/2}^3$  ground states and  $(\pi 1f_{7/2})_{5/2}^3$  excited states in the odd-mass  $_{23}\text{V}$  isotopes. These cluster states were described in detail by Paar [12], and shown to depend on the interaction between the proton cluster and underlying core. In the cases of  $^{51}\text{V}_{28}$  [13] and  $^{55}\text{V}_{32}$  [14, 15], with three protons beyond doubly-magic  $^{48}\text{Ca}_{28}$  and  $^{52}\text{Ca}_{32}$  respectively, the separations between the ground state and  $5/2^-$  cluster states are 320 and 323 keV. However, for  $^{53}\text{V}_{30}$  [16] and  $^{57}\text{V}_{34}$  [17], with three protons beyond  $^{50}\text{Ca}_{30}$  and  $^{54}\text{Ca}_{34}$  respectively, the separations are only 128 and 113 keV, suggesting that the  $^{54}\text{Ca}$  core is more like that of  $^{50}\text{Ca}$  than magic  $^{48}\text{Ca}$  or  $^{52}\text{Ca}$ .

The possible  $N=34$  subshell closure has also been probed by tracking the monopole migration of the  $\nu 1f_{5/2}$  orbital in neighboring nuclei. Previous work by Lidlick *et al.* [18], following the systematic evolution of the  $\nu 1f_{5/2}$  level through consideration of the ground-state spin and parity assignments of odd-odd V and Sc isotopes, indicated an inversion of the  $\nu 1f_{5/2}$  and  $\nu 2p_{1/2}$  single-particle orbitals in moving from the  $_{23}\text{V}$  to the  $_{21}\text{Sc}$

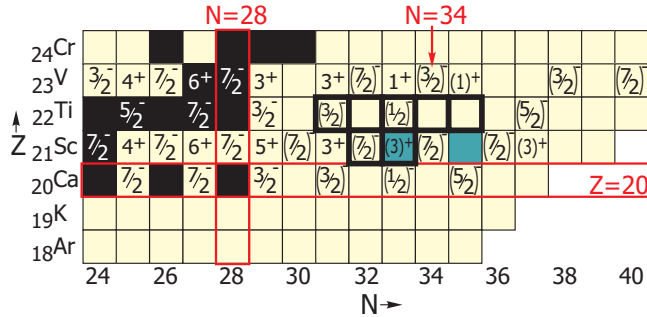


FIG. 1: (Color online) The region of the chart of the nuclides under consideration in the present work. Black squares represent stable nuclei, while nuclei for which low-energy levels were identified in the present work from the  $\beta$  decay of parent nuclei are highlighted by a thick black border. Nuclei for which  $\mu s$  isomeric states permitted access to low-energy levels are shaded. Ground-state spins and parities are included where known, and all even-even nuclides have ground state  $J^\pi = 0^+$ .

isotopes. The apparent close spacing of the  $\nu 1f_{5/2}$  and  $\nu 2p_{1/2}$  orbits in the  $^{22}\text{Ti}$  isotopes, leading to the absence of the  $N=34$  subshell closure for  $Z=22$ , also supports the observed evolution of the neutron single-particle states. Energy spacings between high-spin states in  $^{54}\text{Ti}$  and the first three yrast states in  $^{56}\text{Ti}$  [19] both suggest that the  $\nu 1f_{5/2}$  and  $\nu 2p_{1/2}$  orbitals are nearly degenerate.

Here, we report on the low-energy structures of  $^{53,54}\text{Sc}$  populated following the  $\beta$  decay of  $^{53,54}\text{Ca}$  respectively, as well as on the low-energy levels of  $^{54,56}\text{Sc}$  populated by isomeric  $\gamma$ -ray decay. The low-energy levels of the  $^{21}\text{Sc}$  isotopes can provide insight into the structure of even-even Ca isotopes, as these Sc levels result from the coupling of the odd proton to states in the Ca core. Additionally, we report on newly observed states in  $^{53-57}\text{Ti}$  populated in the  $\beta$  decay of  $^{53-57}\text{Sc}$ , respectively. The nuclei studied in the present work are highlighted in Fig. 1, where known ground-state spins and parities are included for the  $^{20}\text{Ca}$ ,  $^{21}\text{Sc}$ ,  $^{22}\text{Ti}$  and  $^{23}\text{V}$  isotopes. The present results reaffirm the validity of the  $N=32$  subshell closure, and the inversion of the  $\nu 1f_{5/2}$  and  $\nu 2p_{1/2}$  single particle levels moving from the V to the Sc isotopes. However, the apparent compression of the low-energy structure of the neutron-rich Sc isotopes suggests that there may not be a significant  $N=34$  gap between the  $\nu 2p_{1/2}$  and  $\nu 1f_{5/2}$  single-particle states in the  $^{21}\text{Sc}$  isotopic chain.

## II. EXPERIMENTAL PROCEDURE

The  $\beta$  decay and isomeric properties of the neutron-rich  $^{53,54}\text{Ca}$  and  $^{53-57}\text{Sc}$  parent nuclides were deduced in experiments carried out using the experimental facilities at National Superconducting Cyclotron Laboratory (NSCL) at Michigan State University.

A low-energy beam of  $^{76}\text{Ge}^{12+}$  was accelerated to

11.6 MeV/nucleon in the K500 cyclotron, and, following foil stripping to produce  $^{76}\text{Ge}^{30+}$ , accelerated to the full energy of 130 MeV/nucleon in the K1200 cyclotron. The  $^{76}\text{Ge}$  beam was fragmented in a 352-mg/cm<sup>2</sup> thick Be target located at the object position of the A1900 fragment separator [20]. The secondary fragments of interest were selected in the A1900 using a 45-mg/cm<sup>2</sup> Al wedge and 5% momentum slits located at the intermediate dispersive image of the separator.

Fully-stripped secondary fragments were sent to the NSCL Beta Counting System (BCS)[21] located in the S2 experimental vault. The central implantation detector of the BCS was a 995- $\mu\text{m}$  thick double-sided Si microstrip detector (DSSD). The DSSD was segmented into 40 1-mm wide strips in both the horizontal and vertical dimensions, for a total of 1600 pixels. Three Si PIN detectors, with respective thicknesses of 297  $\mu\text{m}$ , 297  $\mu\text{m}$  and 488  $\mu\text{m}$ , were located upstream of the DSSD. Six single-sided Si strip detectors (SSSDs) were placed downstream of the DSSD. The last two SSSDs provided a veto for light particles that arrived at the counting system with the secondary beam. The range of the fragments was adjusted with a 4-mm Al degrader located immediately upstream of the BCS detectors, to implant the ions near the center of the DSSD.

Implanted fragments were unambiguously identified by a combination of multiple energy loss signals, time-of-flight, and the fragment separator magnetic rigidity ( $B\rho$ ) setting. The fragment energy loss was measured in the three PIN detectors, and fragment time-of-flight was determined as the time difference between a particle impinging on a plastic scintillator detector positioned at the dispersive image of the A1900 separator, and the first Si PIN detector (PIN1). Fig. 2 illustrates a representative particle identification spectrum for the experiment investigating  $^{53,54}\text{Ca}$  and  $^{53-56}\text{Sc}$ . The particle ID spectrum that included  $^{57}\text{Sc}$  was presented previously [22]. The secondary beam was defocused to maximize the active area of the DSSD that was illuminated. The average implantation rate over the entire face of the DSSD was  $\leq 100$  Hz.

Fragment- $\beta$  correlations were established in software by requiring a high-energy implantation event in a single pixel  $(x,y)$  of the DSSD, where  $x$  is a horizontal strip and  $y$  is a vertical one. An implantation event was one which had a valid PIN1 signal as well as a high-energy signal in a single strip of both the front and back of the DSSD. A  $\beta$ -decay event was one with a high-gain signal above threshold in the front and back of the DSSD and no signal in PIN1.  $\beta$ -decay events were correlated with implantations only if they occurred in the same pixel, within a specified correlation time window that was adjusted to be at least ten half-lives of the parent nucleus. The differences between the absolute time stamps of correlated  $\beta$  and implantation events were histogrammed to generate decay curves.

The profile of implantations over the DSSD surface was such that pixels near the center of the detector ex-

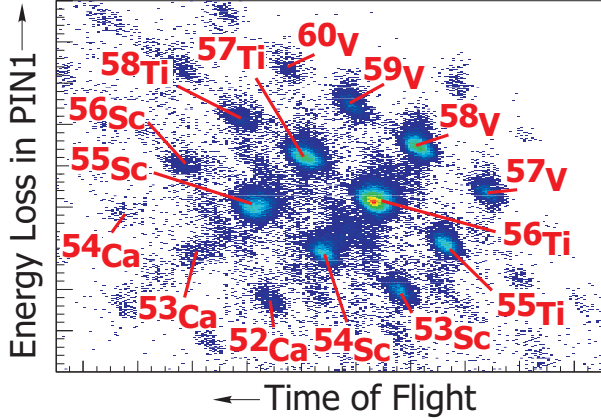


FIG. 2: (Color online) Particle identification spectrum obtained from fragment energy loss in PIN1 versus time-of-flight. A 1900 magnetic rigidity settings of  $B\rho_{1,2} = 4.103$  Tm and  $B\rho_{3,4} = 4.030$  Tm were used to produce the observed cocktail beam.

perienced a significantly higher implantation rate than those at the detector edge. The higher implantation rate led to a larger accumulated activity in the central pixels. To avoid random correlations when using longer correlation times, a subset of pixels on the DSSD was defined for which the time between implantations was  $\geq 100$  s. Corresponding to pixels on the edge of the detector, this subset of pixels included 50% of the detector surface, and was used for the analysis of decays with long correlation times. Details of the correlation times and the pixels used in analysis are included with the results for each nucleus.

Prompt and delayed  $\gamma$ -ray detection was accomplished using sixteen detectors from the Segmented Germanium Array (SeGA) [23]. The Ge detectors were oriented in two concentric rings of 8 detectors each, surrounding the beam pipe containing the BCS detectors. One detector was omitted from the analysis of data for  $^{53,54}\text{Ca}$  and  $^{53-56}\text{Sc}$  due to poor gain stability. A photopeak efficiency for  $\gamma$ -ray detection of 7% at 1 MeV and 3% at 3 MeV was achieved. The energy resolution of all detectors was  $\leq 3.5$  keV for the 1.3-MeV transition in  $^{60}\text{Co}$ . Prompt  $\gamma$  rays emitted following short-lived isomeric decay were detected within a 20- $\mu\text{s}$  window following an implantation event. A time-to-amplitude converter (TAC) was used to measure the time elapsed between an implantation event and the observation of isomeric  $\gamma$  rays in any of the SeGA detectors, permitting measurement of  $\mu\text{s}$  isomer half-lives.

### III. RESULTS

#### A. $^{53}\text{Ca}$ $\beta$ decay

A correlation time of 5 s was used to analyze the  $\beta$  decay of  $^{53}\text{Ca}$  to  $^{53}\text{Sc}$ , where the expected half-life of  $^{53}\text{Ca}$

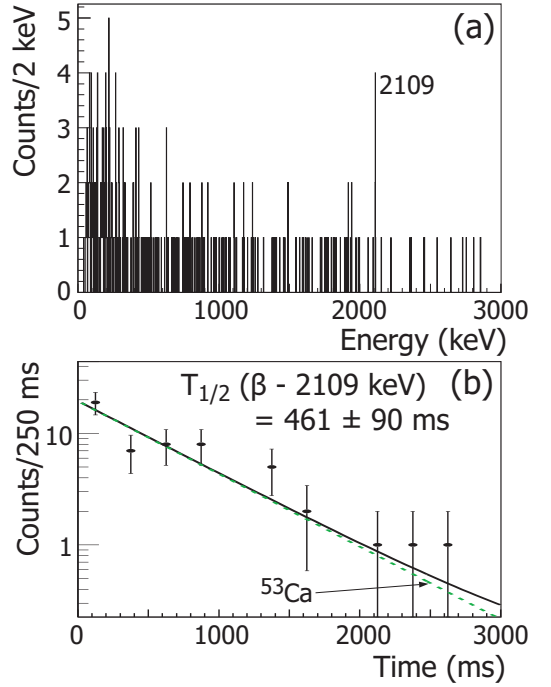


FIG. 3: (a)  $\beta$ -delayed  $\gamma$ -ray spectrum for  $^{53}\text{Ca}$  in the range of 0–3 MeV. The spectrum includes events within the first 5 s following a  $^{53}\text{Ca}$  implantation event, in detector pixels in which the average time between implantations was  $\geq 100$  s. The 2109-keV transition is the sole  $\gamma$  ray observed. (b) Decay curve for  $^{53}\text{Ca}$  using a 5-s correlation time, considering all DSSD pixels, with the additional requirement of a coincident 2109-keV  $\gamma$  ray. The curve was fitted with a single exponential decay.

was on the order of several hundred milliseconds. With a relatively long correlation window, the analysis was restricted to pixels located towards the edge of the implantation DSSD. The  $\beta$ -delayed  $\gamma$ -ray spectrum for  $^{53}\text{Ca}$  in the range 0 to 3 MeV is presented in Fig. 3(a). One transition at  $2109.0 \pm 0.3$  keV has been assigned to the  $\beta$  decay of  $^{53}\text{Ca}$ . The newly-assigned 2109-keV transition was initially reported by us in Ref. [24], and has been recently confirmed in one-proton knockout from  $^{54}\text{Ti}$  [25]. An absolute  $\gamma$  intensity of  $56 \pm 12\%$  was determined for this 2109-keV transition from a Gaussian fit of the peak area, the absolute efficiency of SeGA, and the number of  $\beta$  rays correlated with  $^{53}\text{Ca}$  parent decays. The absolute intensity of this transition suggests that the majority of  $\beta$  intensity from the decay of  $^{53}\text{Ca}$ , excluding the previously established  $40 \pm 10\%$   $\beta n$  branch [26], proceeds through the 2109-keV excited state. This level has been tentatively assigned spin and parity  $3/2^-$ , on the basis of the apparent allowed  $\beta$  decay from a  $(1/2)^-$   $^{53}\text{Ca}$  ground state. The only other possibility for a state populated in allowed  $\beta$  decay is a  $1/2^-$  assignment, which is excluded due to the observed direct transition to the  $7/2^-$   $^{53}\text{Sc}$  ground state.

The decay curve for  $^{53}\text{Ca}$  gated on the 2109-keV transi-

tion is presented in Fig. 3(b). Here, all pixels of the DSSD were considered, since the additional  $\gamma$ -coincidence requirement significantly reduced background events. The data were fitted with a single exponential decay, and a half-life value of  $461 \pm 90$  ms was extracted. This value is higher than the value ( $230 \pm 60$  ms) obtained previously by Mantica *et al.* [22], which was deduced from a half-life curve with no additional  $\gamma$ -ray requirement. The required  $\gamma$  coincidence in the present result eliminates uncertainties arising from daughter decay and background contributions, and provides a more accurate half-life determination. However, as noted in Ref. [22], the possibility of a second  $\beta$ -decaying state in  $^{53}\text{Ca}$  cannot be excluded.

### B. $^{54}\text{Ca}$ $\beta$ decay

Previous measurement of the  $^{54}\text{Ca}$  half-life suggested a value of order 100 ms [22]. With such an expectation, a correlation time of 1 s was used for this short-lived nucleus, and data over the entire surface of the DSSD were considered. The  $\beta$ -delayed  $\gamma$ -ray spectrum of  $^{54}\text{Ca}$  in the range 0 to 1.8 MeV is shown in Fig. 4(a). One transition at  $247.3 \pm 0.3$  keV, with an absolute intensity of  $65 \pm 9\%$ , has been assigned to the  $\beta$  decay of  $^{54}\text{Ca}$ . This transition corresponds to the  $\gamma$  ray observed by Mantica *et al.* [22], and placed as a ground state transition depopulating a 247-keV state in  $^{54}\text{Sc}$ , assigned as  $J^\pi = 1^+$ . Missing  $\beta$  intensity can be attributed to a possible  $\beta n$  branch in the  $^{54}\text{Ca}$  decay.

Fig. 4(b) provides the decay curve obtained by requiring a coincidence with the 247-keV  $\gamma$  ray. This decay curve yielded a half-life value of  $107 \pm 14$  ms, within  $1\sigma$  of the previous value [22].

### C. $^{53}\text{Sc}$ $\beta$ decay

Information regarding the  $\beta$  decay of  $^{53}\text{Sc}$  is sparse. Sorlin *et al.* [27] reported the half-life of  $^{53}\text{Sc}$  as  $> 3$  s, and did not assign  $\gamma$ -ray transitions to the decay. Given the anticipated long half-life, a correlation time of 10 s was used for analysis of this isotope, and only pixels on the edge of the DSSD were considered for the half-life and absolute  $\gamma$ -intensity determinations. On the other hand, the  $\gamma\gamma$  coincidence analysis, which is less sensitive to random background, made use of data from the full DSSD surface. The  $\beta$ -delayed  $\gamma$ -ray spectrum for  $^{53}\text{Sc}$  of Fig. 5(a) contains six transitions, one corresponding to a known  $\gamma$  ray in the decay of the daughter  $^{53}\text{Ti}$  [28], and five assigned to the  $\beta$  decay of  $^{53}\text{Sc}$ . Four additional transitions, not apparent in the spectrum of Fig. 5(a), were identified in the  $\gamma\gamma$  coincidence analysis, and confirmed to be present in the  $\gamma$ -singles spectrum considering data over the full DSSD surface. In the same  $\gamma$ -singles spectrum, two other weak transitions were identified, and assigned to the decay. Transitions observed with energies

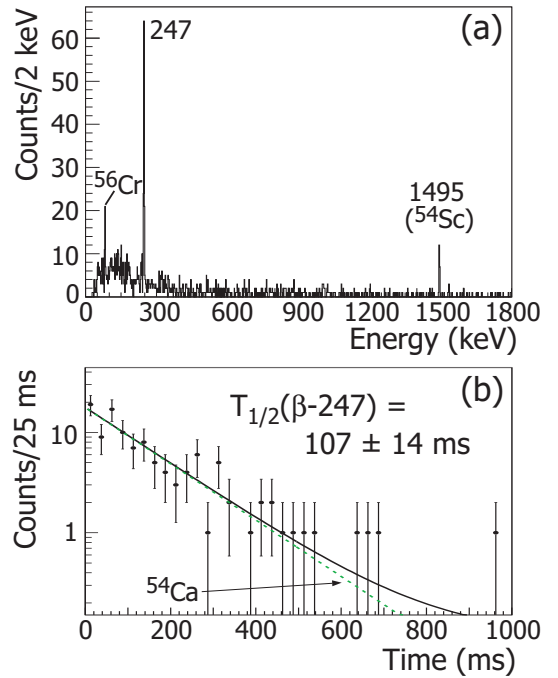


FIG. 4: (Color online) (a)  $\beta$ -delayed  $\gamma$ -ray spectrum for  $^{54}\text{Ca}$  in the range of 0-1.8 MeV. The spectrum includes events within the first 1 s following a  $^{54}\text{Ca}$  implantation. Transitions are marked by their energy in keV. (b) Decay curve for  $^{54}\text{Ca}$ -correlated  $\beta$ -decay events occurring within 1 s of a  $^{54}\text{Ca}$  implantation, with a requirement of a coincident 247-keV  $\gamma$  ray. The curve was fitted with a single exponential decay and a constant background.

of 292, 340, 629, 1237, and 1576 keV agree with those observed in deep-inelastic work on  $^{53}\text{Ti}$  [29].

The decay curve for  $\beta$ -decay events correlated with  $^{53}\text{Sc}$  implantations, with the requirement of a high-energy decay  $\gamma$  ray in coincidence with the decay event, is shown in Fig. 5(b). The use of high-energy  $\gamma$  rays above 1 MeV limited the background contribution. The fit of a single exponential decay to these data yielded a half-life of  $2.4 \pm 0.6$  s.

The proposed decay scheme for levels populated in  $^{53}\text{Ti}$  by the decay of  $^{53}\text{Sc}$  is presented in Fig. 6. The levels at 1237, 1576, 2205 and 2498 keV, and the associated  $\gamma$ -ray transitions were positioned in accord with Ref. [29] and confirmed by  $\gamma\gamma$  coincidence data. The spectrum of  $\gamma$ -ray transitions coincident with the 292-keV transition revealed a new  $\gamma$  ray at  $\sim 413$  keV [see Fig. 7(a)], which was placed in cascade with the 292-keV line, depopulating a new state at 2910 keV. A 701-keV transition was observed in coincidence with the 629-keV line [Fig. 7(d)], which was placed as connecting another new state at 2906 keV with the level at 2205 keV. Both of these transitions, and the corresponding doublet of levels at  $\sim 2910$  keV have been confirmed by Cieplicka *et al.* [30] using Gammasphere data from the reaction  $^{48}\text{Ca} + ^{238}\text{U}$ , which populates states in  $^{53}\text{Ti}$  up to nearly 4 MeV. The

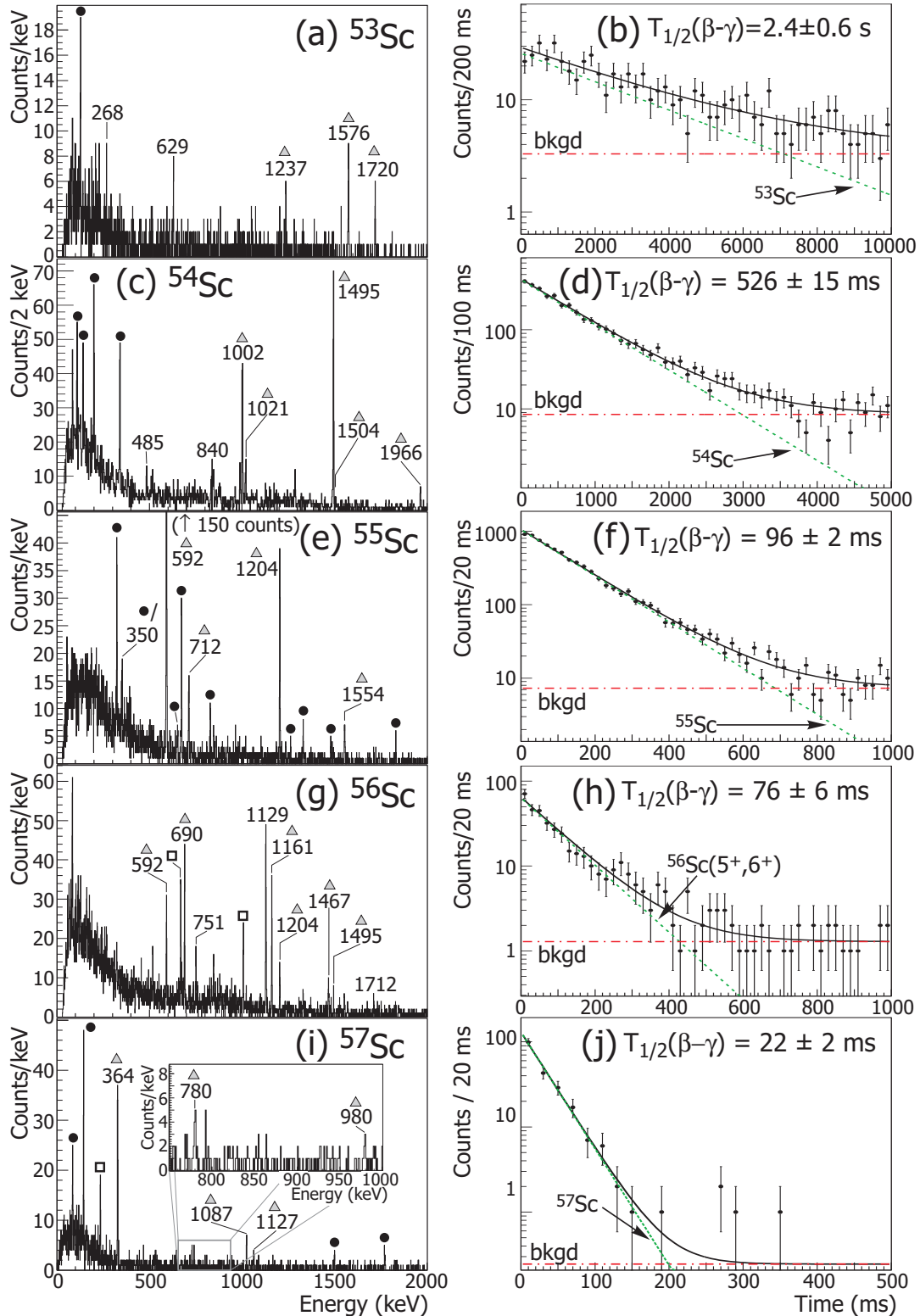


FIG. 5: (Color online)  $\beta$ -delayed  $\gamma$ -ray spectra (left column) and  $\gamma$ -gated half-life curves (right column) for (a, b)  $^{53}\text{Sc}$ , (c, d)  $^{54}\text{Sc}$ , (e, f)  $^{55}\text{Sc}$ , (g, h)  $^{56}\text{Sc}$  and (i, j)  $^{57}\text{Sc}$ . The  $\beta$ -delayed  $\gamma$ -ray spectra cover transitions in the range 0-2 MeV. The conditions under which individual spectra were obtained are discussed in the text. Observed transitions assigned to the decay of the Sc isotopes are marked by their energy in keV. Transitions in the decay of the  $\beta$  daughters are marked by a filled circle, while transitions in decays of the  $\beta$  granddaughters are marked by a hollow square. In (c) and (g), the peak at 83 keV corresponds to a background transition in the  $\beta$  decay of  $^{56}\text{Cr}$ . The half-life curves made use of correlation times specified in the text, and required a coincident  $\gamma$ -ray (marked in the corresponding  $\gamma$  spectrum by a shaded triangle). Data in all cases were fitted with a single exponential decay and a constant background, where such a contribution was non-zero.

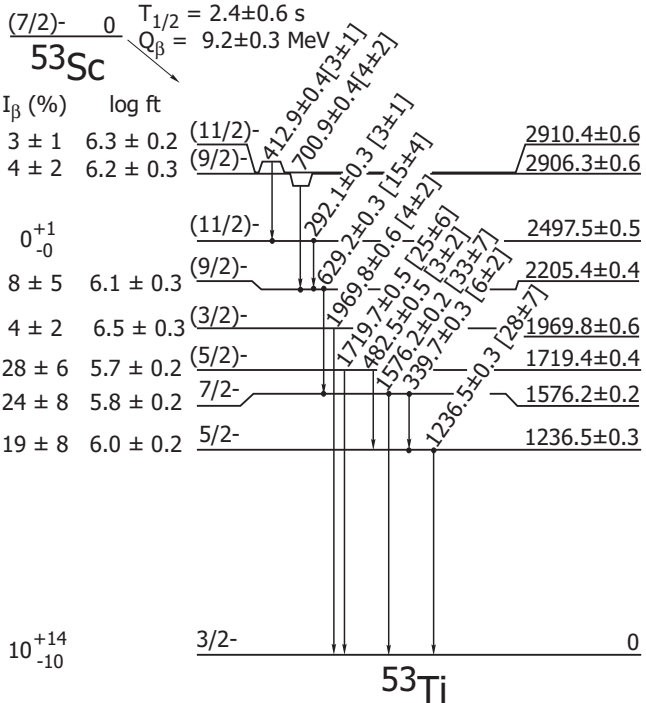


FIG. 6: Proposed decay scheme for the  $\beta$  decay of  $^{53}\text{Sc}$  to states in  $^{53}\text{Ti}$ . The energy of each state is given in keV. The number in brackets following the  $\gamma$ -ray energy is the absolute  $\gamma$ -ray intensity. The decay  $Q$ -value,  $Q_\beta$ , was deduced from data in Ref. [31].

Gammasphere work also confirms the placement of the 483-keV transition connecting the 1719- and 1237-keV levels, and is the source of the precise energy values for the 483- and 1576-keV transitions. The absence of  $\gamma$  rays coincident with the 1720-keV and 1970-keV transitions lead to placement of these transitions feeding the ground state directly. A  $267.6 \pm 0.3$ -keV  $\gamma$  ray (with an absolute intensity of  $6 \pm 3\%$ ) remains unplaced in the  $^{53}\text{Ti}$  level scheme.

Spin and parity assignments proposed in Fig. 6 were adopted from the deep inelastic work of Fornal *et al.* [29], and from comparison of the Gammasphere results with shell-model calculations [30]. All assignments are consistent with the observed  $\beta$  feeding pattern from the  $(7/2)^-$ - $^{53}\text{Sc}$  ground state. The apparent ground-state feeding is consistent with zero.

#### D. $^{54}\text{Sc}$ $\beta$ decay

The analysis of the  $^{54}\text{Sc}$   $\beta$  decay, with a half-life of order  $\sim 400$  ms [18], considered a correlation time of 5 s, again restricted to include pixels towards the edge of the central implantation DSSD. The  $\beta$ -delayed  $\gamma$ -ray spectrum for  $^{54}\text{Sc}$  in the range 0 to 2 MeV is presented in Fig. 5(c). Eleven transitions were identified in this spectrum, and the four lowest in energy were eliminated as candi-

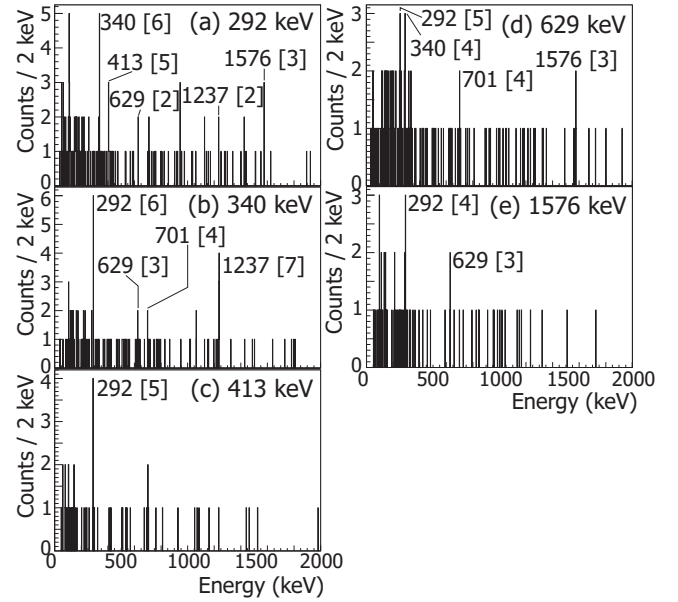


FIG. 7:  $\gamma\gamma$  coincidence spectra gated on the (a) 292-keV, (b) 340-keV, (c) 413-keV, (d) 629-keV, and (e) 1576-keV transitions in coincidence with  $^{53}\text{Sc}$ -correlated  $\beta$ -decay events.  $\gamma$  rays are marked by their energy in keV, the number in square brackets following the energy is the number of counts in the peak. These coincident spectra include data within a 10 s correlation time, for implants collected over the entire surface of the DSSD.

dates for transitions in the  $^{54}\text{Sc}$  decay, based on their apparent half-lives, and likely belong to the decay of the daughter nucleus,  $^{54}\text{Ti}$ .  $\gamma\gamma$  analysis indicates that these four transitions are in coincidence with one another, and the lowest energy transition at 108 keV corresponds to a known transition in  $^{54}\text{V}$  [33]. The remaining seven  $\gamma$  rays were assigned to the  $\beta$  decay of  $^{54}\text{Sc}$ . One additional transition was observed in the  $\gamma$ -spectrum considering data over the entire DSSD surface, and assigned to the decay of  $^{54}\text{Sc}$ . The transitions observed at 1002, 1021 and 1495 keV were previously observed in  $\beta$  decay [18] and deep-inelastic studies [19].

The decay curve of  $^{54}\text{Sc}$ -correlated decay events with the additional requirement of a coincident 1002-, 1021-, 1495-, 1504- or 1966-keV  $\gamma$ -ray transition is given in Fig. 5(d). A fit to these data including a single exponential decay and constant background yielded a half-life for  $^{54}\text{Sc}$  of  $526 \pm 15$  ms, longer than the value of  $360 \pm 60$  ms determined by Liddick *et al.* [18]. The discrepancy between the present value and previous half-life measurements is attributed to the complex deconvolution of the  $\beta$ -decay curve. A new half-life of  $2.1 \pm 1.0$  s was determined here for the daughter  $^{54}\text{Ti}$ , which is slightly longer than the literature value [32]. Additionally, missing  $\beta$  intensity is suggestive of a neutron-branching contribution of  $16 \pm 9\%$ . Inclusion of these factors in fitting a  $\beta$ -decay curve impacts the fit to data. The additional  $\gamma$ -ray coincidence condition taken here permits a half-life determi-

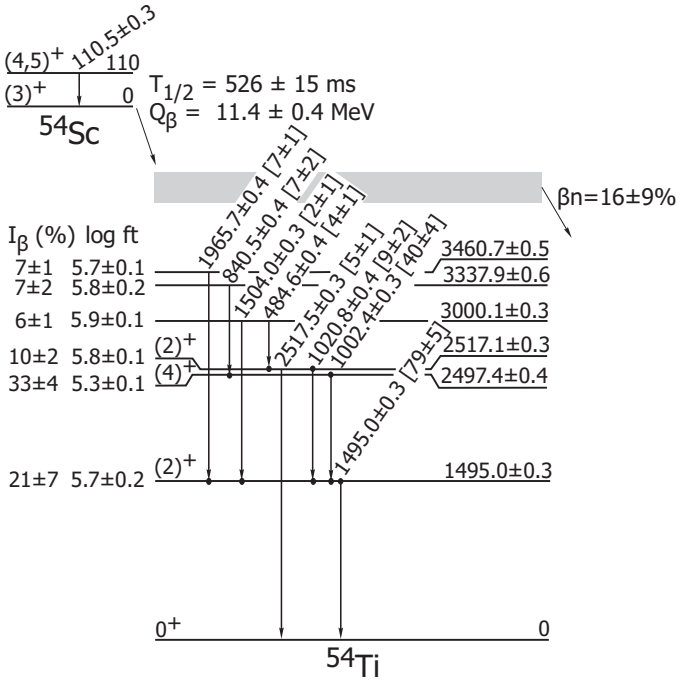


FIG. 8: Proposed decay scheme for  $^{54}\text{Sc}$  to states in  $^{54}\text{Ti}$ . The energy of each state is given in keV. The number in brackets following the  $\gamma$ -ray decay energy is the absolute  $\gamma$ -ray intensity. The  $Q_\beta$  value was deduced from data in Ref. [31].

nation that requires only two parameters, and extraction of a more accurate value.

The proposed decay scheme for  $^{54}\text{Sc}$  to levels in  $^{54}\text{Ti}$  is shown in Fig. 8. Placement of the 1002-, 1021- and 1495-keV transitions follows assignments made in previous works [18, 19]. The new transitions at 485, 840, 1504 and 1966 keV were placed based on  $\gamma\gamma$  coincidences. Energy-sum relationships were used to place the 1504-keV cross-over transition connecting the states at 3000 and 1495 keV, and the 2517-keV cross-over transition connecting the state at 2517 keV with the ground state.

Apparent  $\beta$  feedings and  $\log ft$  values deduced from the absolute  $\gamma$  intensities are included in Fig. 8. The  $J^\pi$  of the  $^{54}\text{Sc}$  ground state was previously limited to  $(3,4)^+$  [18]. Apparent  $\beta$  feeding is observed to both the  $2_1^+$  and  $4_1^+$  states previously identified in Ref. [19], at 1495 and 2497 keV respectively. The suggested allowed decay to both of these states further restricts the spin and parity for the  $^{54}\text{Sc}$  ground state to  $3^+$ . No feeding is expected to the  $0^+ {^{54}\text{Ti}}$  ground state according to the selection rules for allowed  $\beta$  decay, assuming a  $J^\pi = 3^+$  ground state for  $^{54}\text{Sc}$ .  $J^\pi$  values for the states with energy 1495, 2497 and 2517 keV were adopted from previous works [18, 19]. Apparent allowed  $\beta$  feeding from the  $(3)^+ {^{54}\text{Sc}}$  ground state limits the spin and parity of the newly placed levels at 3000, 3338 and 3461 keV to  $J^\pi = 2^+, 3^+$ , or  $4^+$ .

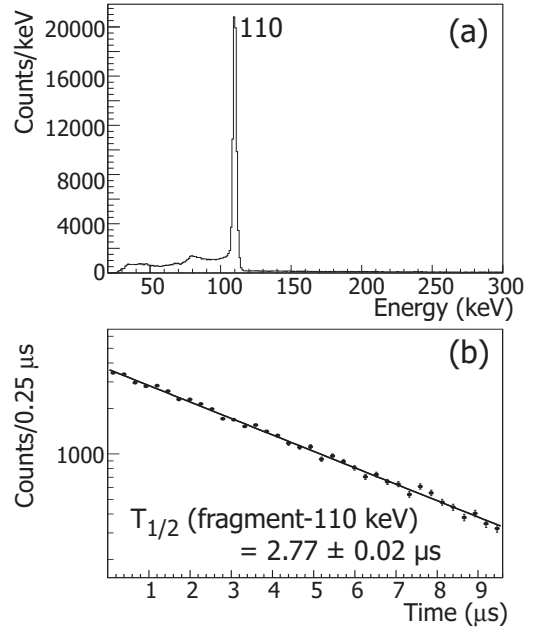


FIG. 9: (a)  $\gamma$ -ray spectrum collected within a  $20\text{-}\mu\text{s}$  window following a  $^{54}\text{Sc}$  implant. The 110-keV isomeric transition observed here was previously reported in Ref. [33], and confirmed in Ref. [18]. (b) Time dependence of the 110-keV transition. The decay curve was fitted with a single exponential decay to yield a half-life of  $2.77 \pm 0.02 \mu\text{s}$ .

### E. $^{54}\text{Sc}$ isomeric decay

The isomeric  $\gamma$ -ray spectrum collected within  $20 \mu\text{s}$  of a  $^{54}\text{Sc}$  implantation event is presented in Fig. 9(a). The 110-keV isomeric transition was initially reported by Grzywacz *et al.* [33], and assigned E2 multipolarity. The transition was observed here with high statistics, and an improved half-life of  $2.77 \pm 0.02 \mu\text{s}$  was deduced [Fig. 9(b)]. This more precise value is consistent with the result of Grzywacz *et al.*, and an E2 multipolarity assignment based on comparison to Weisskopf lifetime estimates. Based on the  $(3)^+$  spin and parity of the  $^{54}\text{Sc}$  ground state and an E2 isomeric transition, the limits on  $J^\pi$  for the 110-keV level are  $J^\pi = 1^+$  or  $5^+$ .  $J = 1$  is excluded as this state was not directly populated following the  $\beta$  decay of  $^{54}\text{Ca}$ . Thus, under the assumption of an E2 multipolarity for the transition, the 110-keV isomeric state in  $^{54}\text{Sc}$  is tentatively assigned a spin and parity of  $5^+$ , as originally suggested by Grzywacz *et al.* [33]. However, this assignment assumes a single-particle nature for the final and initial states. More complicated wavefunctions, involving configuration mixing, open the window for a  $4^+$  spin and parity assignment for the 110-keV isomeric state. This possibility is explored further in Section IV.B.

### F. $^{55}\text{Sc}$ $\beta$ decay

A correlation time of 1 s was used for the analysis of events associated with  $^{55}\text{Sc}$ , based on previous half-life measurements [18, 22, 27] indicative of a  $\sim 100$  ms half-life. Analysis of the  $\beta$ -gated  $\gamma$ -ray spectrum was again restricted to pixels towards the edge of the central implantation DSSD. The spectrum in the range of 0 to 2 MeV is given in Fig. 5(e). A total of 13  $\gamma$ -ray transitions were identified in this spectrum; of these, 9 correspond to known  $\gamma$  rays in the decay of the daughter isotope,  $^{55}\text{Ti}$ . The remaining 4 transitions have been assigned to the  $\beta$  decay of  $^{55}\text{Sc}$ . One peak in the  $\gamma$ -singles spectrum, at  $349.6 \pm 0.7$  keV, is very broad, and is likely a doublet. A known transition in the  $\beta$  decay of  $^{55}\text{Ti}$ , with energy  $349.3 \pm 0.6$  keV, may contribute to this peak. The transition with energy 592 keV corresponds to the  $\gamma$  ray previously observed in the  $\beta$  decay of  $^{55}\text{Sc}$  by Liddick *et al.* [18]. States in  $^{55}\text{Ti}$  have been studied by deep inelastic scattering with Gammasphere at the ATLAS facility [15]. The  $\gamma$  rays reported here with energies 350, 592, 1204 and 1554 keV agree with transitions observed in that work.

A summed decay curve from gates on the  $\gamma$  rays in  $^{55}\text{Ti}$  with energies 592, 712, 1204 and 1554 keV is given in Fig. 5(f). This curve was fitted with a single exponential decay and constant background, and the resulting half-life of  $96 \pm 2$  ms is consistent with previous measurements [18, 22].

The level scheme for  $^{55}\text{Ti}$  populated following  $\beta$  decay of  $^{55}\text{Sc}$  is illustrated in Fig. 10. Placement of the 350-, 592-, 1204- and 1554-keV transitions is based on previous deep inelastic results [15], which established the yrast level structure for  $^{55}\text{Ti}$  up to  $J^\pi = (19/2)^-$ . One additional transition, not seen in Ref. [15], with energy 712 keV was observed in coincidence with the 1204- and 592-keV transitions. This 712-keV transition was placed depopulating a new state with energy 2508 keV.

Tentative  $J^\pi$  values were assigned for the ground state and excited states at 592, 1796 and 2146 keV in Ref. [15], based on comparisons to shell model calculations with the GXPF1A interaction [11]. The assignments proposed in that work included  $J^\pi = 1/2^-$  for the  $^{55}\text{Ti}$  ground state, which has recently been confirmed by a one-neutron knockout measurement from  $^{56}\text{Ti}$  to states in  $^{55}\text{Ti}$  performed at GSI [34]. Such a  $J^\pi$  assignment would exclude allowed  $\beta$  decay from the  $^{55}\text{Sc}$  ground state populating the  $^{55}\text{Ti}$  ground state directly. Thus, the missing  $\beta$  intensity of  $17 \pm 7\%$  suggests the possible presence of a  $\beta n$  branch in the  $^{55}\text{Sc}$  decay. Absence of transitions in  $^{54}\text{Ti}$  (see Fig. 8) in the  $\beta$ -delayed  $\gamma$ -ray spectrum may indicate that the  $\beta n$  branch mainly populates the  $^{54}\text{Ti}$  ground state directly. The spin and parity assignments proposed by Zhu *et al.* [15] are adopted here. Apparent allowed  $\beta$  decay to the newly placed state at 2508 keV limits this state to  $J^\pi = 5/2^-, 7/2^-$  or  $9/2^-$ .

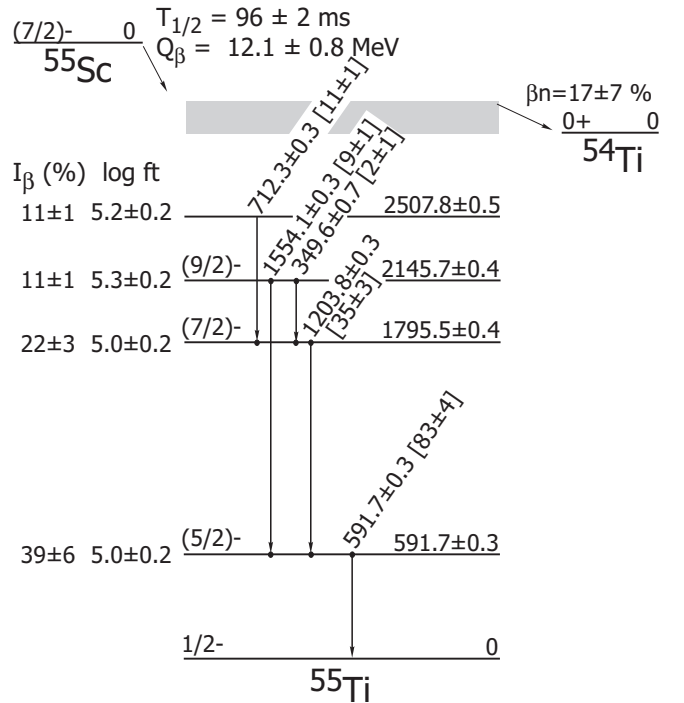


FIG. 10: Decay scheme for  $^{55}\text{Sc}$  to states in  $^{55}\text{Ti}$ .

### G. $^{56}\text{Sc}$ $\beta$ decay

Analysis of the  $\beta$  decay of  $^{56}\text{Sc}$  was completed using a correlation time of 1 s, and the full DSSD surface was considered. The  $\beta$ -delayed  $\gamma$ -ray spectrum for  $^{56}\text{Sc}$  in the range of 0 to 2 MeV can be found in Fig. 5(g), where nine transitions have been assigned to the decay of  $^{56}\text{Sc}$ , and are summarized in Table I. Two additional transitions were assigned to the decay of the granddaughter nuclide,  $^{56}\text{V}$ . The transitions with energies 592, 690, 751, 1129 and 1161 keV were previously observed in both  $\beta$  decay [18] and deep-inelastic experiments [19]. It was noted in Ref. [18] that the transition with energy  $592.3 \pm 0.5$  keV was within the error of a known transition in  $^{55}\text{Ti}$ , and the possibility of  $\beta$ -delayed neutron emission was suggested. Another known transition in  $^{55}\text{Ti}$ , at 1204 keV [15] is also present in the delayed  $\gamma$ -ray spectrum for  $^{56}\text{Sc}$ , confirming  $\beta$ -delayed neutron emission in this decay.

Liddick *et al.* [18] proposed two  $\beta$ -decaying states in  $^{56}\text{Sc}$ : a low-spin state with  $T_{1/2} = 35 \pm 5$  ms, and a higher-spin level with slightly longer  $T_{1/2} = 60 \pm 7$  ms. Given the different spin values, the two  $\beta$ -decaying states were observed to populate different levels in the  $^{56}\text{Ti}$  daughter. Gated decay curves were generated for each  $\gamma$ -ray transition identified in Fig. 5(g), and fitted with a single exponential decay and constant background. The resultant half-life values are summarized in Table I. Values deduced from the decay curves gated on the 690- and 1161-keV  $\gamma$  rays, which depopulate levels at 2979 and 2289 keV respectively, are in agreement with the previ-

TABLE I: Energies and relative intensities of  $\beta$ -delayed  $\gamma$  rays assigned to the decay of  $^{56}\text{Sc}$ . Observed half-lives for  $\gamma$ -gated decay curves are also included.

$E_\gamma$ (keV)	$I_\gamma^{absolute}$ (%)	Decay Mode	Initial State (keV)	Final State (keV)	$T_{1/2}$ (ms)
$591.7 \pm 0.3$	$14 \pm 2$	$\beta\text{n}$	592	0	$78 \pm 25$
$689.6 \pm 0.3$	$18 \pm 2$	$\beta$	2979	2289	$73 \pm 10$
$750.9 \pm 0.4$	$8 \pm 2$	$\beta$	1880	1129	$24 \pm 7$
$1128.7 \pm 0.3$	$48 \pm 4$	$\beta$	1129	0	$51 \pm 6$
$1160.6 \pm 0.3$	$30 \pm 3$	$\beta$	2289	1129	$78 \pm 9$
$1203.5 \pm 0.3$	$8 \pm 1$	$\beta\text{n}$	1796	592	$68 \pm 19$
$1466.8 \pm 0.3$	$6 \pm 1$	$\beta$	-	-	$60 \pm 13$
$1494.8 \pm 0.3$	$3 \pm 1$	$\beta$	4474	2979	$150 \pm 44$
$1711.6 \pm 0.3$	$3 \pm 1$	$\beta$	-	-	$29 \pm 10$

ous half-life determination for the higher-spin isomer [18]. The transitions assigned to the  $\beta\text{n}$  decay also have half-lives consistent with decay from the higher-spin state, as do the transitions with energies 1467 and 1495 keV. The weighted average of the half-lives for transitions populated solely by the higher-spin isomer is  $75 \pm 6$  ms.

The half-life of the lower-spin,  $\beta$ -decaying state [18] was previously deduced from a two-component fit to the decay curve gated on the 1129-keV  $\gamma$  transition, which depopulates a state fed by both  $\beta$ -decaying states in  $^{56}\text{Sc}$ . Two newly-identified  $\gamma$ -ray transitions at 751 and 1712 keV decay with half-lives similar to that extracted for the lower-spin isomer. These  $\gamma$  rays apparently depopulate states fed exclusively by the lower-spin isomer. The weighted average of the half-lives for the 751- and 1712-keV transitions yields a half-life for the lower-spin isomer of  $26 \pm 6$  ms.

Levels in  $^{56}\text{Ti}$  and  $^{55}\text{Ti}$  populated in the decay of the two  $\beta$ -decaying states in  $^{56}\text{Sc}$  are shown in Fig. 11. States in  $^{55}\text{Ti}$  are known from the present  $^{55}\text{Sc}$   $\beta$ -decay results, previous  $\beta$ -decay studies [18], and deep-inelastic work [15]. The three states at 1129, 2289 and 2979 keV in  $^{56}\text{Ti}$  were previously identified and assigned tentative spin and parity values [18, 19], which were adopted in Fig. 11. Observed  $\gamma\gamma$  coincidences between the 1129- and 751-keV transitions suggest the placement of an additional state populated by the lower-spin  $\beta$ -decaying state at 1880 keV. In addition to populating the two states at 2289 and 2979 keV directly, observed  $\gamma\gamma$  coincidences between the 1495- and 690-keV transitions suggest that the higher-spin  $\beta$ -decaying state populates a level at 4474 keV. Only the 1467- and 1712-keV  $\gamma$  transitions remain unplaced in the present level scheme for  $^{56}\text{Ti}$ .

Absolute  $\gamma$ -ray intensities were determined for the  $\beta$ -delayed  $\gamma$ -ray transitions in the  $^{56}\text{Sc}$  decay by comparison of the number of observed  $\gamma$  rays, adjusted for the absolute efficiency of SeGA, with the number of observed  $^{56}\text{Sc}$  decays. The number of parent decays in this case was determined using the total number of implantations, taken from the particle identification, and the average  $\beta$ -

detection efficiency of  $11.4 \pm 0.4\%$ . The absolute  $\gamma$ -ray intensities are included in Table I, and in the decay scheme of Fig. 11. Apparent  $\beta$  branches were deduced from the absolute  $\gamma$ -ray intensities. Decay from the higher-spin isomer apparently populates both the  $4^+$  and  $6^+$  states in  $^{56}\text{Ti}$ . This suggests that the higher-spin isomer has  $J^\pi = 5^+$ , in contradiction to the previous assignment of  $(6,7)^+$  by Liddick *et al.* [18]. However, the large  $Q_\beta$  value for the decay allows the  $(4)^+$  state at 2289 keV to be populated by cascades from above, resulting in the observed intensity difference between the 690- and 1161-keV transitions. Given this possibility, the higher-spin  $\beta$ -decaying state has been tentatively assigned as  $(5,6)^+$ . The state with an energy of 4474 keV, also populated by the higher-spin  $\beta$ -decaying state, has  $J^\pi$  limited to  $4^+$ ,  $5^+$ ,  $6^+$  or  $7^+$ , depending on the spin and parity of the higher-spin  $\beta$ -decaying state in  $^{56}\text{Sc}$ .

Decay from the lower-spin  $\beta$ -decaying state in  $^{56}\text{Sc}$  apparently directly feeds the first excited  $2^+$  state in  $^{56}\text{Ti}$ , which limits the spin and parity of this  $\beta$ -decaying state to  $1^+$ ,  $2^+$  or  $3^+$ . The  $J^\pi$  for the  $^{56}\text{Sc}$  ground state can be further restricted if there is direct  $\beta$  feeding to the  $^{56}\text{Ti}$  ground state. The absolute intensity of the 592-keV transition in the  $\beta\text{n}$  daughter  $^{55}\text{Ti}$  suggests a lower-limit for the neutron branching ratio of  $14 \pm 2\%$ . Even under the assumption that the two unplaced  $\gamma$  transitions directly populate the  $^{56}\text{Ti}$  ground state, there is  $29 \pm 7\%$  of the  $\beta$  intensity unaccounted for. Two scenarios can account for the missing intensity: either direct feeding to the  $^{56}\text{Ti}$  ground state or  $\beta\text{n}$  decay populating the ground state of  $^{55}\text{Ti}$  directly. These possibilities were investigated by reanalyzing the  $\beta$  decay of  $^{56}\text{Sc}$  with the longer correlation time of 5 s. With a longer correlation time, it was possible to compare the intensities of  $\gamma$ -ray transitions in the decay of the  $\beta\text{n}$  daughter  $^{55}\text{Ti}$  (672.5 keV,  $I_\gamma^{absolute} = 44 \pm 4\%$  [14]), and the  $\beta\beta$  granddaughter  $^{56}\text{V}$  (668.4 keV,  $I_\gamma^{absolute} = 26 \pm 2\%$  [35]). The ratio of  $\beta$  to  $\beta\text{n}$  decays in  $^{56}\text{Sc}$  can be determined by the ratio of the intensities of the 668- and 673-keV transitions, which are detected with nearly the same efficiency in SeGA. Approximately 70% of the decays of  $^{56}\text{Sc}$  populate states in  $^{56}\text{Ti}$ . Thus, the missing  $\beta$  intensity cannot be fully accounted for by  $\beta\text{n}$  decay to the ground state of  $^{55}\text{Ti}$ , and there is apparent direct population of the  $0^+$   $^{56}\text{Ti}$  ground state, which must be from the lower-spin  $\beta$ -decaying state. This suggests a spin and parity for the lower-spin  $\beta$ -decaying state of  $J^\pi = 1^+$ . Direct feeding from the  $(1)^+$   $\beta$ -decaying state limits  $J^\pi$  of the state at 1880 keV to  $(0,1,2)^+$ .

## H. $^{56}\text{Sc}$ isomer decay

The isomeric  $\gamma$ -ray spectrum collected within a  $20\text{-}\mu\text{s}$  time window following a  $^{56}\text{Sc}$  implantation is presented in Fig. 12(a). Five transitions were observed. Those with energies 140, 188 and 587 keV were previously reported by Liddick *et al.* [18].

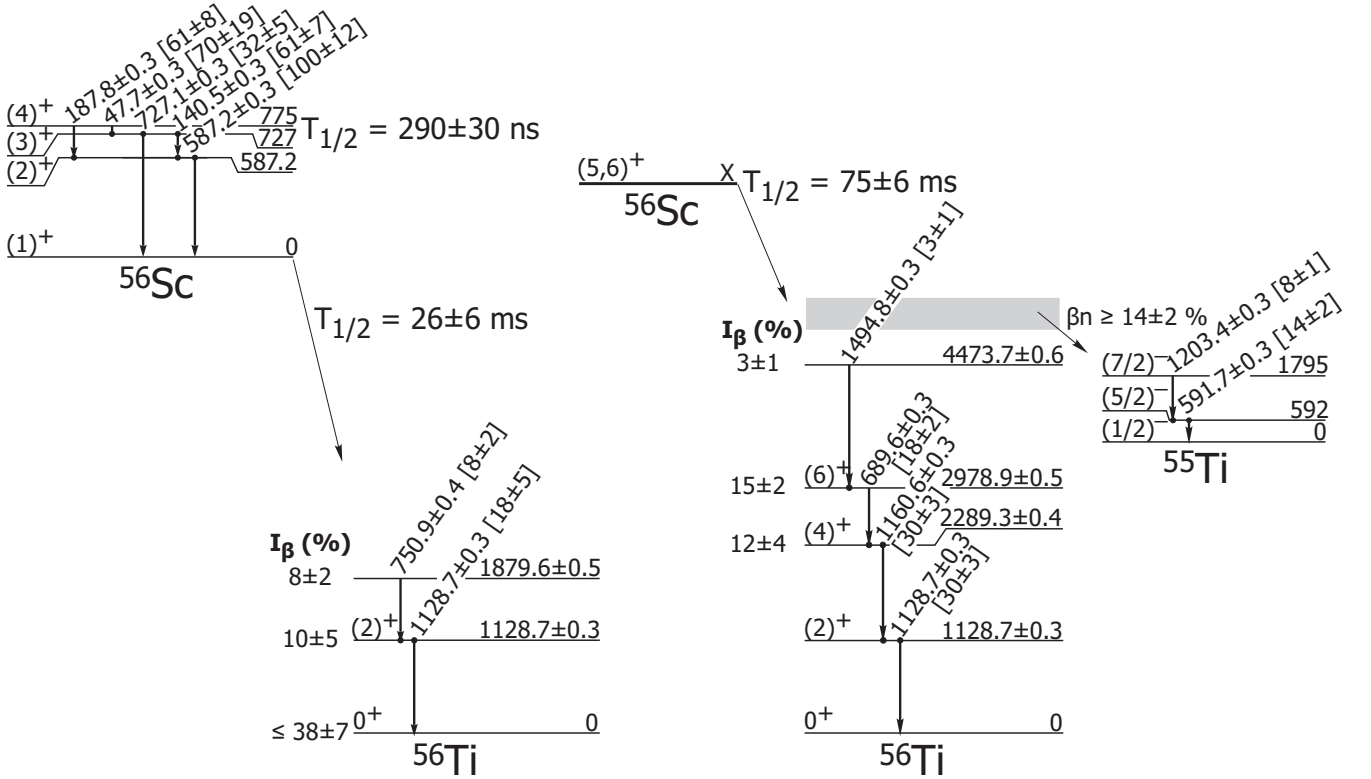


FIG. 11: Proposed level scheme for  $^{56}\text{Sc}$ , following the  $\gamma$  decay of the isomeric transition at 775 keV, and levels in  $^{55,56}\text{Ti}$  populated following  $\beta$ -decay of  $^{56}\text{Sc}$ . The number in brackets following the isomeric  $\gamma$ -ray energies are the relative  $\gamma$  intensities. The numbers following the  $\beta$ -delayed  $\gamma$ -ray energies are the absolute  $\gamma$ -ray intensities. The relative energies of the two  $\beta$ -decaying states is not known. The energy of the higher-spin  $\beta$ -decaying state, denoted by “X” may be negative.  $Q_\beta$  for this decay is  $13.7 \pm 0.7$  MeV [31].

The observed  $\gamma$ -ray energy as a function of the time elapsed between a  $^{56}\text{Sc}$  implantation event and prompt  $\gamma$  emission is presented in Fig. 12(b). The five transitions appear to decay with the same half-life. The projection of Fig. 12(b) onto the time axis, gated on the five isomeric transitions, is included in Fig. 12(c). The resultant decay curve was fitted with a single exponential decay and a constant background, resulting in a half-life of  $290 \pm 30$  ns.

The low-energy structure of  $^{56}\text{Sc}$ , populated by isomeric decay (as presented in Fig. 11), was based on observed  $\gamma\gamma$  coincidences (see Fig. 13), as well as relative intensity and energy-sum relationships.

A novel approach was taken to determine which of the two  $\beta$ -decaying states in  $^{56}\text{Sc}$  is populated in the isomeric decay from the 775-keV level. A half-life curve was constructed considering only  $\beta$ -decay events correlated with  $^{56}\text{Sc}$  implantation events that were in turn correlated with one of the five prompt  $\gamma$  rays. The resultant decay curve is presented in Fig. 14. The deduced short half-life of  $30 \pm 5$  ms provides evidence that the isomeric transitions populate the lower-spin  $\beta$ -decaying state.

The tentative spin and parity assignment of the lower-spin  $\beta$ -decay isomer in  $^{56}\text{Sc}$  as  $1^+$  permits tentative  $J^\pi$  assignments to the remaining levels populated in decay of the isomeric state in  $^{56}\text{Sc}$ . The 188-keV transition, which

directly depopulates the isomeric level, is proposed to be of E2 character, based on the comparison to Weisskopf half-life estimates, and the competing 48-keV transition to be of the M1 type. It follows that the 140-keV transition must also have M1 multipolarity. The observed intensities of the 727-keV and 140-keV transitions then suggest the former  $\gamma$  ray to be an E2 transition. Finally, the remaining 587-keV transition must have M1 multipolarity. These assignments lead to the tentatively assigned  $J^\pi = 2^+, 3^+$  and  $4^+$  values for the states in  $^{56}\text{Sc}$  with energies 587, 727 and 775 keV above the lower-spin  $\beta$ -decaying state respectively, again assuming that this state in  $^{56}\text{Sc}$  has  $J^\pi = 1^+$  quantum numbers.

## I. $^{57}\text{Sc}$ $\beta$ decay

$^{57}\text{Sc}$  was studied in a separate experiment from that used to deduce the results for the isotopes previously discussed. However, the decay of  $^{57}\text{Sc}$  to states in  $^{57}\text{Ti}$  was analyzed in a similar manner. A correlation time of 500 ms was used for the analysis of this decay, which had a previous half-life measurement of order tens of milliseconds. Pixels over the entire DSSD surface were considered in the analysis.

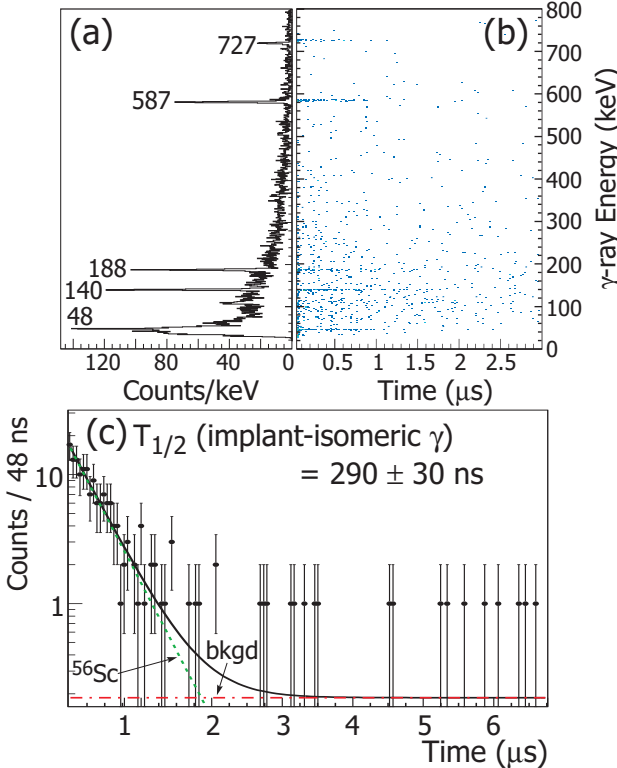


FIG. 12: (Color online) (a) The prompt  $\gamma$ -ray spectrum collected within the first 20  $\mu$ s following a  $^{56}\text{Sc}$  implant. The  $\gamma$  rays assigned to the isomer decay in  $^{56}\text{Sc}$  are marked by their energies in keV. The additional peak visible in the spectrum at 110 keV is contamination from the isomer decay of  $^{54}\text{Sc}$ . (b) A plot of  $\gamma$ -ray energy as a function of time elapsed after the corresponding  $^{56}\text{Sc}$  implantation event. The five isomer  $\gamma$  lines are visible, decaying with comparable lifetimes. (c) A projection of (b) onto the time axis, gated on the five identified  $\gamma$ -ray transitions. The resultant decay curve was fitted with a single exponential decay and constant background.

The  $\beta$ -delayed  $\gamma$ -ray spectrum for the decay of  $^{57}\text{Sc}$  is presented in Fig. 5(i). Four transitions in this spectrum were attributed to the  $\beta$  decay of the  $^{57}\text{Ti}$  daughter nucleus, and one transition was known from the  $\beta$  decay of the  $^{57}\text{V}$  granddaughter. The remaining five  $\gamma$  rays in Fig. 5(i) were attributed to the  $\beta$  decay of  $^{57}\text{Sc}$ , and are listed in Table II. No previous information on  $\beta$ -delayed  $\gamma$  rays in  $^{57}\text{Sc}$  is available from the literature. The transition at 1127 keV is close in energy to a known transition in  $^{56}\text{Ti}$ , at  $1128.7 \pm 0.3$  keV [18, 19], and may suggest a  $\beta$ -delayed neutron branch from  $^{57}\text{Sc}$  to levels in  $^{56}\text{Ti}$ .

The decay curve for  $^{57}\text{Sc}$ -correlated  $\beta$  decays with the additional requirement of a decay  $\gamma$ -ray coincidence is given in Fig. 5(j). The decay curve was fitted with a single exponential decay and a constant background, and the deduced half-life was  $22 \pm 2$  ms. The new half-life value is slightly longer than the previous  $^{57}\text{Sc}$  half-life measurement of  $13 \pm 4$  ms [36], which did not include a  $\gamma$ -ray tag.

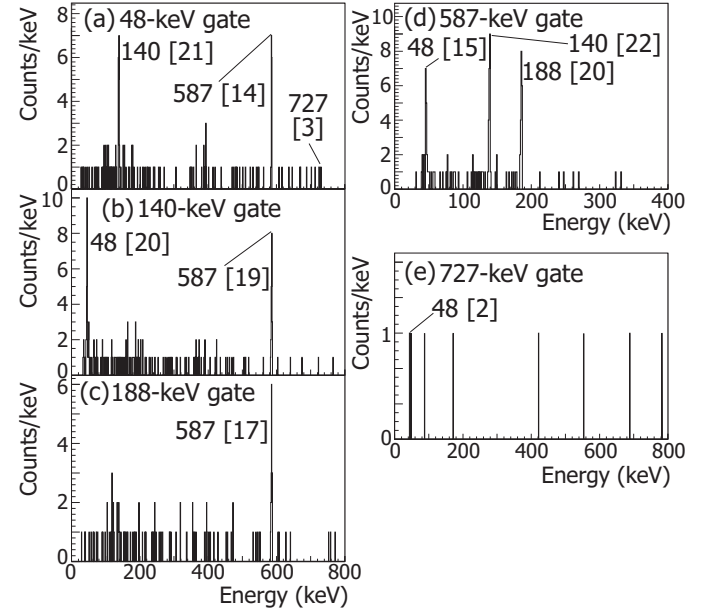


FIG. 13:  $\gamma\gamma$  coincidence gates for the (a) 48-keV, (b) 140-keV, (c) 188-keV, (d) 587-keV and (e) 727-keV transitions in the 20- $\mu$ s time window following a  $^{56}\text{Sc}$  implant.  $\gamma$  rays are marked by their energy in keV and the number in square brackets is the number of counts in the peak.

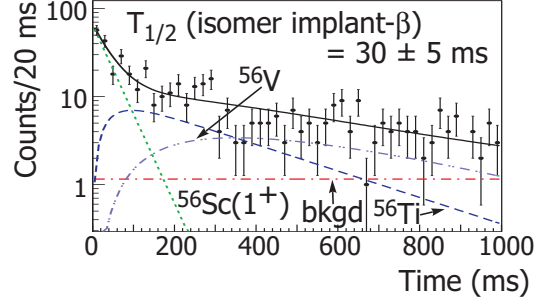


FIG. 14: (Color online) Decay curve for  $^{56}\text{Sc}$ -correlated  $\beta$  decays considering only  $^{56}\text{Sc}$  implants coincident with identified isomeric  $\gamma$ -ray transitions. The decay curve is fitted with a single exponential decay and a constant background, and includes contributions from the growth and decay of the  $\beta$ -decay daughter ( $^{56}\text{Ti}$ ,  $T_{1/2} = 200 \pm 5$  ms [14]) and granddaughter ( $^{56}\text{V}$ ,  $T_{1/2} = 216 \pm 4$  ms [35]).

TABLE II: Energies and absolute intensities of  $\beta$ -delayed  $\gamma$  rays assigned to the decay of  $^{57}\text{Sc}$ .

$E_\gamma(\text{keV})$	$I_\gamma^{\text{abs}} (\%)$
$364.2 \pm 0.4$	$76 \pm 8$
$780.4 \pm 0.5$	$9 \pm 3$
$979.6 \pm 0.5$	$5 \pm 1$
$1087.1 \pm 0.4$	$21 \pm 3$
$1127.1 \pm 0.5$	$12 \pm 2$

No  $\gamma\gamma$  coincidence data were available due to low

statistics. The absolute intensity for the 364-keV  $\gamma$  ray suggests that it directly populates the  $^{57}\text{Ti}$  ground state, and it has been placed as a ground-state transition. No other conclusions regarding the low energy structure of  $^{57}\text{Ti}$  could be drawn from the present data.

#### IV. DISCUSSION

The low-energy levels of the  $_{21}\text{Sc}$  isotopes can be discussed, in the context of the extreme single-particle model, as a coupling of the odd  $1f_{7/2}$  proton to the states in the  $_{20}\text{Ca}$  core isotopes. The success or failure of simple coupling schemes in explaining the low-energy structure of the Sc isotopes can also provide indirect indications regarding the presence or absence of subshell closures in the Ca core nuclei. The structure of the Sc isotopes is first discussed in the framework of this coupling, and then compared to the results of shell model calculations. Results in the Ti isotopes are discussed in terms of the systematic evolution of structure along the  $Z=22$  isotopic chain.

##### A. Low-energy structure of $^{53}\text{Sc}$

The low-energy structure of  $^{53}\text{Sc}$  can be interpreted as a weak coupling of the valence  $1f_{7/2}$  proton to states in  $^{52}\text{Ca}$ , which, assuming a robust  $N=32$  subshell closure, can be viewed as a doubly magic core [4, 24]. Coupling of the valence proton to the first  $2^+$  state in  $^{52}\text{Ca}$  should produce a quintet of states in  $^{53}\text{Sc}$  with  $J^\pi$  values ranging from  $3/2^-$  to  $11/2^-$ , at energies centered around  $\sim 2.6$  MeV. Studies of  $^{53}\text{Sc}$  via deep inelastic reactions [37] have populated  $9/2^-$  and  $11/2^-$  states near this energy, which are likely members of the  $\pi 1f_{7/2} \otimes 2^+$  multiplet. The  $\beta$  decay of  $^{53}\text{Ca}$  was observed to populate only one state in  $^{53}\text{Sc}$ . The population of a single state in the decay of  $^{53}\text{Ca}$  decay limits the spin and parity of the  $^{53}\text{Ca}$  ground state to  $J^\pi=1/2^-$ , as allowed  $\beta$  decay from a  $J^\pi=3/2^-$  or  $5/2^-$   $^{53}\text{Ca}$  ground state would be expected to populate several levels of the  $\pi 1f_{7/2} \otimes 2^+$  multiplet. The single new level at 2109 keV populated in the decay from a  $J^\pi=1/2^-$   $^{53}\text{Ca}$  ground state is a likely candidate for the  $3/2^-$  member of the  $\pi 1f_{7/2} \otimes 2^+$  multiplet. The three known levels in  $^{53}\text{Sc}$  (see Fig. 15) reside at just over 2 MeV, nearly the energy expected within the weak coupling framework. The success of this scheme in describing the structure of  $^{53}\text{Sc}$  provides further support for the robust nature of the  $N=32$  subshell closure in the  $_{20}\text{Ca}$  isotopes.

##### B. Low-energy structure of even- $A$ Sc isotopes

The structure of the even- $A$   $_{21}\text{Sc}$  isotopes can be described in terms of coupling of the valence  $1f_{7/2}$  proton

$(2)+$	$2562$	$(11/2)-$	$2617$
		$(9/2)-$	$2283$
$\pi f_{7/2} \otimes 52\text{Ca}(2^+)$		$(3/2)-$	$2109$
$0+$	$0$	$(7/2)-$	$0$
$52\text{Ca}$		$53\text{Sc}$	

FIG. 15: The comparison of the known levels in  $^{53}\text{Sc}$  [24, 37] to states in  $^{52}\text{Ca}$  suggests that  $^{53}\text{Sc}$  is accurately described by weak coupling of the odd  $\pi 1f_{7/2}$  proton to the  $^{52}\text{Ca}$  core.

particle with  $2p_{3/2}$ ,  $2p_{1/2}$ ,  $1f_{5/2}$ , and at higher energies,  $1g_{9/2}$ , valence neutron structures to states in a corresponding  $_{20}\text{Ca}$  core. This is shown most directly by considering the cases of  $^{50}\text{Sc}$  and  $^{52}\text{Sc}$ , where this simple description explains many aspects of the known low-energy structures.

$^{50}\text{Sc}$  has one proton and one neutron particle outside of the doubly magic  $^{48}\text{Ca}$  core, and the lowest energy levels can be described in terms of the coupling of a valence  $1f_{7/2}$  proton and  $2p_{3/2}$  neutron. The low-energy structure, known from  $\beta$  decay [38], transfer reactions [39], and charge exchange reactions [40] can be seen in Fig. 16(a). The four states lowest in energy arise from the configuration  $(\pi 1f_{7/2})^1 \otimes (\nu 2p_{3/2})^1$ , which produces four states ranging from  $J^\pi = 2^+$  to  $5^+$ . The particle-particle coupling rules [41] suggest that the states in this multiplet are arranged in a downward-opening parabola, in good agreement with the experimental energy levels. Promotion of the valence neutron in  $^{50}\text{Sc}$  to the  $\nu 2p_{1/2}$  level will give the configuration  $(\pi 1f_{7/2})^1 \otimes (\nu 2p_{1/2})^1$ , producing two states with  $J^\pi = 3^+$ ,  $4^+$ . Two  $3^+$  states are identified in the level scheme of  $^{50}\text{Sc}$  above 2 MeV, and either may be a candidate for the  $3^+$  member of this doublet. The energy spacing between multiplets arising from configurations involving the  $\nu 2p_{3/2}$  and  $\nu 2p_{1/2}$  states is directly related to the  $\nu 2p_{3/2}$ - $\nu 2p_{1/2}$  single-particle spacing, and thus the  $\nu 2p_{3/2}$ - $\nu 2p_{1/2}$  spin-orbit splitting. The apparent separation of these two multiplets in  $^{50}\text{Sc}$  is of order 2 MeV, a gap sufficient to account for the established  $N=32$  subshell closure in  $_{21}\text{Sc}$ .

The low-energy structure of  $^{52}\text{Sc}$  can be similarly described in terms of coupling of a valence  $1f_{7/2}$  proton particle and  $2p_{3/2}$  neutron hole, taking  $^{52}\text{Ca}$  as the inert core. States in this odd-odd nucleus have been identified following  $\beta$  decay [3], in-beam  $\gamma$ -ray spectroscopy following secondary fragmentation [42] and deep-inelastic work [37, 43]. The known levels are presented in Fig. 16(b). As discussed in Refs. [37, 43], the lowest-lying quartet of states in  $^{52}\text{Sc}$  can be associated with the configuration  $(\pi 1f_{7/2})^1 \otimes (\nu 2p_{3/2})^{-1}$ . The four states with

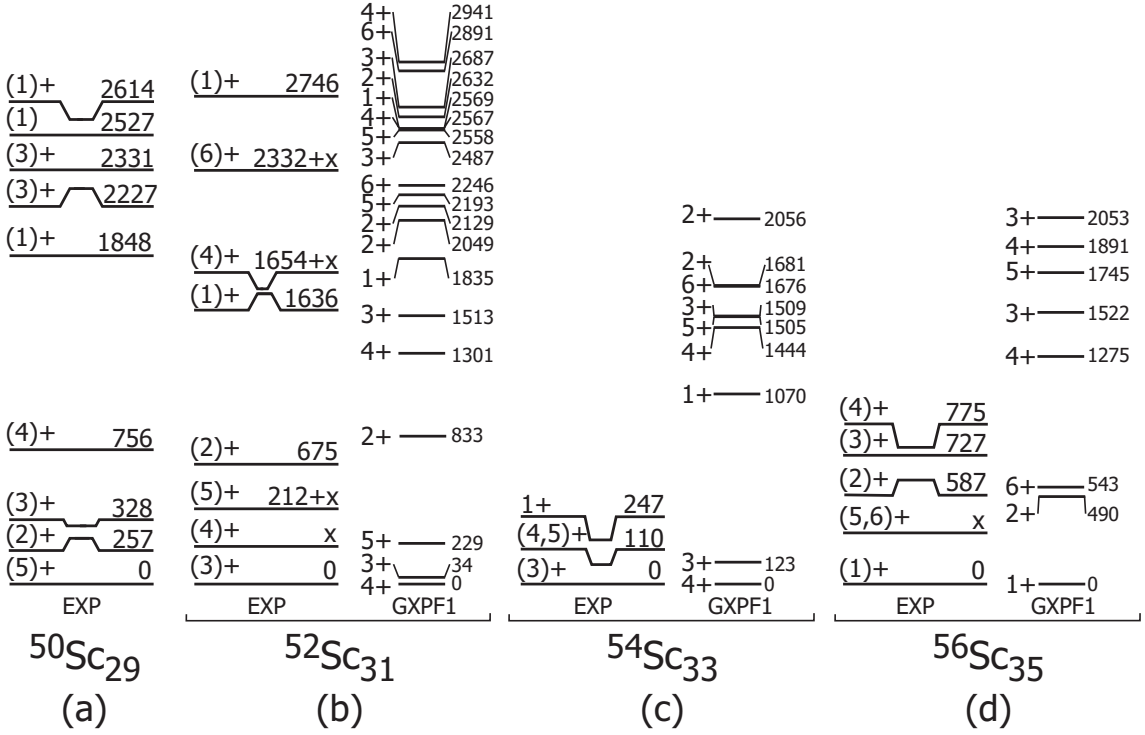


FIG. 16: Experimentally determined levels below 3 MeV for the odd-odd, even-A (a)  $^{50}\text{Sc}$ , (b)  $^{52}\text{Sc}$ , (c)  $^{54}\text{Sc}$  and (d)  $^{56}\text{Sc}$  isotopes. Level energies are labeled in keV. Theoretical predictions using the GXPF1 shell-model interaction are shown where available.

$J^\pi=2^+-5^+$  should form an upward-opening parabola, since the coupling involves a proton particle and neutron hole. Shell-model calculations based on the effective interactions GXPF1 [4] and GXPF1A [43], which assume an inert  $^{48}\text{Ca}$  core, both result in the near-degeneracy of the  $3^+$  and  $4^+$  states of this multiplet. The energy separation between these states has not been established experimentally, but is likely small. The success of the Pandya transformation [44] in relating the particle-particle  $(\pi 1f_{7/2})^1 \otimes (\nu 2p_{3/2})^1$  states of  $^{50}\text{Sc}$  to the particle-hole  $(\pi 1f_{7/2})^1 \otimes (\nu 2p_{3/2})^{-1}$  states in  $^{52}\text{Sc}$  also suggests that the energy separation between the  $3^+$  and  $4^+$  states is small in  $^{52}\text{Sc}$ , and that the configurations of these low-lying levels in both nuclei is fairly pure. Calculations using the GXPF1 effective interaction [4] confirm the configurational purity of the four lowest-energy levels. The coupling of the  $1f_{7/2}$  proton to an excited  $2p_{1/2}$  neutron to give a pair of states with  $J^\pi=3^+, 4^+$  accounts for the observed  $4^+$  state in  $^{52}\text{Sc}$  at  $\sim 1.7$  MeV. The  $6^+$  state at  $\sim 2.3$  MeV in  $^{52}\text{Sc}$  has been shown in shell-model calculations to have parentage including this configuration, though the extent of this contribution varies between shell-model interactions. Calculations using the GXPF1A interaction [43] suggest that the primary parentage of the 2.3-MeV  $6^+$  state is  $(\pi 1f_{7/2})^1 \otimes [\nu(2p_{3/2}^2 2p_{1/2}^1)]$ , while the  $(\pi 1f_{7/2})^1 \otimes [\nu(2p_{3/2}^2 1f_{5/2}^1)]$  configuration is predicted to

dominate the first  $8^+$  state in  $^{52}\text{Sc}$ , experimentally observed at  $\sim 3.6$  MeV [43]. The energy separation between states arising from the  $(\pi 1f_{7/2})^1 \otimes (\nu 2p_{3/2})^{-1}$  and  $(\pi 1f_{7/2})^1 \otimes [\nu(2p_{3/2}^2 2p_{1/2}^1)]$  configurations was  $\sim 2$  MeV, corresponding to the spin-orbit splitting between the  $\nu 2p_{3/2}$  and  $\nu 2p_{1/2}$  single-particle states, in agreement with the situation in  $^{50}\text{Sc}$ . As noted by Fornal *et al.* [43], the apparent separation between the  $\nu 2p_{1/2}$  and  $\nu 1f_{5/2}$  single-particle states, as inferred from the energy spacing between the  $6^+$  and  $8^+$  states in  $^{52}\text{Sc}$ , is slightly smaller than that predicted in the GXPF1A interaction.

The low-energy structure of  $^{54}\text{Sc}$ , with two additional neutrons, should exhibit significant change. The  $\nu 2p_{3/2}$  orbital is now fully occupied, and the  $^{54}\text{Sc}$  structure at low energy should reflect coupling of the valence  $1f_{7/2}$  proton particle to either a  $2p_{1/2}$  or  $1f_{5/2}$  neutron, taking  $^{52}\text{Ca}$  as the inert core. The  $\nu 2p_{1/2}$  single-particle level is expected to lie below the  $\nu 1f_{5/2}$  state for the  $^{54}\text{Sc}$  isotopes, based on the observations in  $^{52}\text{Sc}$ . Assuming such an ordering, the  $(\pi 1f_{7/2})^1 \otimes (\nu 2p_{1/2})^1$  coupling yields a doublet of states with  $J^\pi=3^+, 4^+$ , which is expected to be lowest in energy in  $^{54}\text{Sc}$ . Shell model results [18] predict the  $3^+$  and  $4^+$  states of this configuration to be close in energy, and thus the spin and parity of the  $^{54}\text{Sc}$  ground state from a theory perspective is not clear. The ground state is tentatively assigned  $J^\pi=3^+$  in the present work. Considering the situation in terms of

the coupling, it may be natural to assume that the isomeric 110-keV level corresponds to the  $4^+$  state arising from the  $(\pi 1f_{7/2})^1 \otimes (\nu 2p_{1/2})^1$  configuration. However, within the simple coupling framework it is difficult to accept an in-multiplet M1 transition hindered so strongly as to yield the experimental isomer half-life of  $2.8 \mu\text{s}$ . In this case, the two excited states identified in  $^{54}\text{Sc}$ , the isomeric  $(5)^+$  level and higher-lying  $1^+$  state, may be explained as arising from the configuration  $(\pi 1f_{7/2})^1 \otimes (\nu 1f_{5/2})^1$ . This coupling results in a sextet of states ranging from  $J^\pi=1^+$  to  $6^+$ . The particle-particle coupling would produce a downward-facing parabola. There are, however, inconsistencies in the experimental level ordering in  $^{54}\text{Sc}$  when compared with shell model calculations. The  $1^+$  state lies above the  $5^+$  state in energy in the level scheme as presented in Fig. 16(c), a result which is inconsistent with calculations using the GXPF1 effective interaction. An alternative  $J^\pi$  assignment for the states in  $^{54}\text{Sc}$  with a  $4^+$  ground state and  $6^+$  110-keV isomeric level is a possibility, but the placement of the  $6^+$  level below the  $1^+$  level is also unexpected. The apparent experimental level ordering would be explained if the  $(\pi 1f_{7/2})^1 \otimes (\nu 2p_{3/2})^{-1}$  configuration was the origin of the  $3^+$  and  $5^+$  states. However, as the  $\nu 2p_{3/2}-\nu 2p_{1/2}$  spin-orbit splitting is a fairly constant  $\sim 2$  MeV, this multiplet is expected at much higher excitation energy in  $^{54}\text{Sc}$ , making this possibility unlikely.

An alternative to the  $5^+$  assignment for the 110-keV isomeric state is a  $4^+$  assignment. While not expected based on comparison of the deduced isomer lifetime with Weisskopf single-particle estimates, which favor an E2 multipolarity for the 110-keV transition, a  $4^+$  spin and parity cannot be excluded for the 110-keV state. Calculations using the GXPF1 [9], GXPF1A [11] and KB3G [45] interactions all predict a doublet of states near the  $^{54}\text{Sc}$  ground state with  $J^\pi=3^+$  and  $4^+$ . The transition probabilities,  $B(M1 : 3^+ \rightarrow 4^+)$  and  $B(E2 : 3^+ \rightarrow 4^+)$  calculated with these three interactions are shown in Table III, along with the calculated partial half-lives. In all cases, the M1 component would dominate the transition. However, the  $B(M1 : 3^+ \rightarrow 4^+)$  values are small, giving rise to half-lives of order nanoseconds or longer – much slower than the picoseconds expectation from the single-particle Weisskopf estimate. The  $B(M1 : 3^+ \rightarrow 4^+)$  value is very sensitive to the degree of mixing in the wavefunctions for the  $3^+$  and  $4^+$  states. With increased configuration mixing, there is increased suppression of the  $B(M1 : 3^+ \rightarrow 4^+)$  value, hindering the transition. A  $4^+$  spin and parity assignment is in better agreement with the expectation for the level ordering in  $^{54}\text{Sc}$ . However, more work is required to make a firm spin assignment for the 110-keV isomeric state in  $^{54}\text{Sc}$ .

The  $1^+$  state at energy 247 keV in  $^{54}\text{Sc}$  can only be explained by the  $(\pi 1f_{7/2})^1 \otimes (\nu 1f_{5/2})^1$  configuration. Even if this is the only member of the multiplet identified, the energy separation between the ground state with  $(\pi 1f_{7/2})^1 \otimes (\nu 2p_{1/2})^1$  and the excited states from  $(\pi 1f_{7/2})^1 \otimes (\nu 1f_{5/2})^1$  appears to be small. Shell model

results using the GXPF1 effective interaction [18] predict a  $\nu 2p_{1/2}-\nu 1f_{5/2}$  separation of more than 1 MeV, which manifests itself in  $^{54}\text{Sc}$  as an expanded low-energy level structure [see Fig. 16(c)]. The compression observed here between multiplets arising from coupling with the  $\nu 2p_{1/2}$  and  $\nu 1f_{5/2}$  neutron states suggests a  $\nu 2p_{1/2}-\nu 1f_{5/2}$  single-particle energy separation smaller than that assumed in the GXPF1 Hamiltonian, and is possibly inconsistent with a robust  $N=34$  subshell closure.

Another rapid structure change should be evident in  $^{56}\text{Sc}$ . The addition of two neutrons to  $^{54}\text{Sc}$  should fill the  $\nu 2p_{1/2}$  single-particle orbital. The unpaired valence neutron will then occupy the  $1f_{5/2}$  state. Under this assumption, the lowest energy states in  $^{56}\text{Sc}$  are expected to arise from the  $(\pi 1f_{7/2})^1 \otimes (\nu 1f_{5/2})^1$  configuration. The resulting sextet of states with  $J^\pi=1^+$  to  $6^+$  should be arranged in a downward facing parabola, with the  $4^+$  state at the vertex. The challenge in comparing expectations in  $^{56}\text{Sc}$  to the new data is the unknown position of the higher-spin  $\beta$ -decaying state, relative to the low-energy structure established by the isomer decay. However, the states at low energy in  $^{56}\text{Sc}$  with  $J^\pi=1^+$ ,  $2^+$  and  $(5,6)^+$  are difficult to explain in a simple way outside of the  $(\pi 1f_{7/2})^1 \otimes (\nu 1f_{5/2})^1$  configuration. The  $3^+$  and  $4^+$  states cannot be trivially assigned the same configuration, as they may also arise from the  $(\pi 1f_{7/2})^1 \otimes (\nu 2p_{1/2})^1$  coupling, depending on the relative position of the  $\nu 2p_{1/2}$  and  $\nu 1f_{5/2}$  single-particle orbitals. In fact, significant mixing would be expected between the  $3^+$ / $4^+$  states in the  $\pi 1f_{7/2}-\nu 1f_{5/2}$  and  $\pi 1f_{7/2}-\nu 2p_{1/2}$  multiplets. This mixing is already reflected in the GXPF1 calculated levels, even with a large  $\nu 2p_{1/2}-\nu 1f_{5/2}$  gap.

### C. Systematic variation of the Ti levels

The experimentally-known levels below 4 MeV in the odd- $A$  neutron-rich  $^{53,55,57}_{22}\text{Ti}$  isotopes are represented in Fig. 17. The levels of the  $^{22}\text{Ti}$  isotopes have been well characterized [5, 7, 15, 19, 29] by the GXPF1A [11] shell-model effective interaction.

Within the GXPF1A interaction, the ordering of the neutron single-particle states places the  $2p_{1/2}$  orbital below the  $1f_{5/2}$  orbital for the Ti isotopes. Given such an ordering,  $^{55}\text{Ti}_{33}$  is expected to have a  $1/2^-$  ground state, as the first neutron above the  $N=32$  subshell closure should occupy the  $2p_{1/2}$  orbital. The first excited state in  $^{55}\text{Ti}$  then corresponds to excitation of the valence neutron into the  $1f_{5/2}$  orbital. The recent direct determination of the ground state spin and parity in  $^{55}\text{Ti}$  [34] provides confirmation for the ordering of the  $\nu 2p_{1/2}$  and  $\nu 1f_{5/2}$  orbitals, with the  $\nu 2p_{1/2}$  orbital lying lower in energy, similar to the ordering in the  $^{21}\text{Sc}$  isotopes. Thus, it appears that the  $\nu 2p_{1/2}-\nu 1f_{5/2}$  level ordering changes already in going from  $^{23}\text{V}$  to  $^{22}\text{Ti}$ , though a significant energy gap between these orbitals is not present in the Ti isotopes [15].

TABLE III: Calculated transition probabilities and half-lives for the transition between the  $3^+$  and  $4^+$  states in  $^{54}\text{Sc}$ , using the GXPF1, GXPF1A and KB3G shell-model effective interactions. The Weisskopf single-particle estimates for the half-life of a 110-keV transition are also included.

	GXPF1	GXPF1A	KB3G	Single-Particle
$B(M1 : 3^+ \rightarrow 4^+) (\mu_N^2)$	0.02611	0.00369	0.00080	
$T_{1/2}(M1) (\text{s})$	$8.10 \times 10^{-10}$	$1.56 \times 10^{-8}$	$8.94 \times 10^{-7}$	$9.30 \times 10^{-12}$
$B(E2 : 3^+ \rightarrow 4^+) (e^2 \text{fm}^4)$	5.07	6.24	6.96	
$T_{1/2}(E2) (\text{s})$	$4.05 \times 10^{-6}$	$1.72 \times 10^{-5}$	$1.03 \times 10^{-3}$	$2.89 \times 10^{-6}$

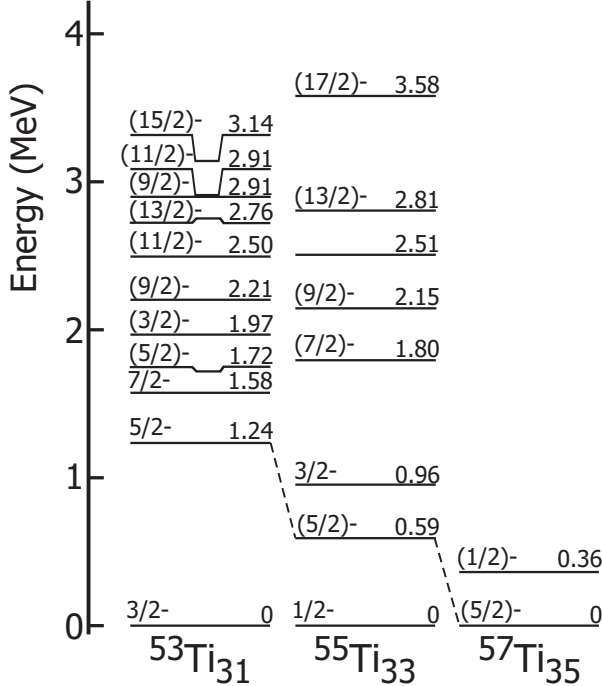


FIG. 17: Experimentally-determined levels below 4 MeV for odd- $A$   $^{53,55,57}\text{Ti}$  isotopes.

Based on the assumed neutron-level ordering,  $^{57}\text{Ti}_{35}$  is expected to have a  $5/2^-$  ground state, with a neutron configuration of  $2p_{3/2}^4 2p_{1/2}^2 1f_{5/2}^1$ , and a first excited state with  $J^\pi=1/2^-$ , corresponding to excitation of a  $2p_{1/2}$  neutron into the  $1f_{5/2}$  orbital. Thus, this is essentially an inversion of the two lowest states in  $^{55}\text{Ti}$ . Calculations with the GXPF1A interaction have placed this first excited state at an energy of 422 keV [17]. In the present results, one state has been placed in the level scheme of  $^{57}\text{Ti}$  at an energy of 364 keV, which may correspond to the  $1/2^-$  first excited state. If this is the case,  $\beta$  decay from the  $^{57}\text{Sc}$   $7/2^-$  ground state should not directly populate this state, and it must be fed indirectly from higher-lying states. However, the 364-keV transition is much stronger than the other transitions observed in the decay, and direct feeding cannot be excluded. Allowed  $\beta$  decay from  $^{57}\text{Sc}$ , with a  $7/2^-$  ground state, populating the first-excited state in  $^{57}\text{Ti}$  would suggest a reversal of the level ordering shown in Fig. 17, and would present a

significant challenge for theory. However, before the origin of the 364-keV state can be confirmed, a more complete picture of the low-energy states in  $^{57}\text{Ti}$  is required.

## V. SUMMARY

The low-energy levels of neutron-rich  $^{53,54,56}\text{Sc}$  and  $^{53-57}\text{Ti}$  have been investigated through the  $\beta$  decay of the parent nuclides  $^{53,54}\text{Ca}$  and  $^{53-57}\text{Sc}$ , as well as through prompt isomeric  $\gamma$ -ray emission from  $^{54,56}\text{Sc}$ . The low-energy structures of the Sc isotopes can be considered in the extreme single-particle model as the result of coupling of the valence  $1f_{7/2}$  proton to states in the corresponding  $^{20}\text{Ca}$  core. Such a description works well in  $^{53}\text{Sc}$ , where the valence proton weakly couples to states in doubly-magic  $^{52}\text{Ca}_{32}$ . The success of this description provides further evidence for the validity of the  $N=32$  subshell closure in the Ca isotopes. Interpretation of the low-energy levels in the even- $A$  Sc isotopes as resulting from the simple coupling of a  $1f_{7/2}$  proton and valence neutrons to a Ca core provides preliminary information regarding the energy separation between neutron single-particle levels. While more work is required to complete the relevant multiplets of states, early indications suggest that the low-energy levels in the Sc isotopes are compressed, and that a significant  $N=34$  subshell gap does not exist between the  $2p_{1/2}$  and  $1f_{5/2}$  neutron levels in the  $^{21}\text{Sc}$  isotopes. More information is required in the  $^{20}\text{Ca}$  isotopes to determine conclusively whether the removal of the final  $1f_{7/2}$  proton is sufficient to create a substantial subshell closure at  $N=34$ .

## Acknowledgments

The authors thank the NSCL operations staff for providing the primary and secondary beams for this experiment and NSCL  $\gamma$  group for assistance setting up the Ge detectors from SeGA. This work was supported in part by the National Science Foundation under Grant No. PHY-06-06007 and by the U.S. Department of Energy, Office of Nuclear Physics, under contracts No. DE-AC02-06CH11357 (ANL) and DEFG02-94ER40834 (University of Maryland) and by the Polish Scientific Committee grant 1PO3B 059 29. HLC and GFG would like to acknowledge support from the Natural Science and

Engineering Research Council (NSERC) of Canada.

---

[1] M.G. Mayer and J.H.D. Jensen, *Elementary Theory of Nuclear Shell Structure*, Wiley, New York, 1955.

[2] T. Otsuka, R. Fujimoto, Y. Utsuno, B.A. Brown, M. Honma and T. Mizusaki, *Phys. Rev. Lett.* **87**, 082502 (2001).

[3] A. Huck, G. Klotz, A. Knipper, C. Miehé, C. Richard-Serre, G. Walter, A. Poves, H.L. Ravn and G. Marguier, *Phys. Rev. C* **31**, 2226 (1985).

[4] A. Gade, R.V.F. Janssens, D. Bazin, R. Broda, B.A. Brown, C.M. Campbell, M.P. Carpenter, J.M. Cook, A.N. Deacon, D.-C. Dinca, B. Fornal, S.J. Freeman, T. Glasmacher, P.G. Hansen, B.P. Kay, P.F. Mantica, W.F. Mueller, J.R. Terry, J.A. Tostevin and S. Zhu, *Phys. Rev. C* **74**, 021302(R) (2006).

[5] R.V.F. Janssens, B. Fornal, P.F. Mantica, B.A. Brown, R. Broda, P. Bhattacharyya, M.P. Carpenter, M. Cincausero, P.J. Daly, A.D. Davies, T. Glasmacher, Z.W. Grabowski, D.E. Groh, M. Honma, F.G. Kondev, W. Królas, T. Lauritsen, S.N. Liddick, S. Lunardi, N. Marginear, T. Mizusaki, D.J. Morrissey, A.C. Morton, W.F. Mueller, T. Otsuka, T. Pawlat, D. Seweryniak, H. Schatz, A. Stolz, S.L. Tabor, C.A. Ur, G. Viesti, I. Wiedenhöver and J. Wrzesiński, *Phys. Lett. B* **546**, 55 (2002).

[6] J.I. Prisciandaro, P.F. Mantica, B.A. Brown, D.W. Anthony, M.W. Cooper, A. Garcia, D.E. Groh, A. Komives, W. Kumarasiri, P.A. Lofy, A.M. Oros-Peusquens, S.L. Tabor and M. Wiedeking, *Phys. Lett. B* **510**, 17 (2001).

[7] D.-C. Dinca, R.V.F. Janssens, A. Gade, D. Bazin, R. Broda, B.A. Brown, C.M. Campbell, M.P. Carpenter, P. Chowdhury, J.M. Cook, A.N. Deacon, B. Fornal, S.J. Freeman, T. Glasmacher, M. Honma, F.G. Kondev, J.-L. Lecouey, S.N. Liddick, P.F. Mantica, W.F. Mueller, H. Olliver, T. Otsuka, J.R. Terry, B.A. Tomlin and K. Yoneda, *Phys. Rev. C* **71**, 041302(R) (2005).

[8] A. Bürger, T.R. Saito, H. Grawe, H. Hübel, P. Reiter, J. Gerl, M. Górska, H.J. Wollersheim, A. Al-Khatib, A. Banu, T. Beck, F. Becker, P. Bednarczyk, G. Benzoni, A. Bracco, S. Brambilla, P. Bringel, F. Camera, E. Clément, P. Doornenbal, H. Geissel, A. Görzen, J. Grębosz, G. Hammond, M. Hellström, M. Honma, M. Kavatsyuk, O. Kavatsyuk, M. Kmiecik, I. Kojouharov, W. Korten, N. Kurz, R. Lozeva, A. Maj, S. Mandal, B. Million, S. Muralithar, A. Neusser, F. Nowacki, T. Otsuka, Zs. Podolyák, N. Saito, A.K. Singh, H. Weick, C. Wheldon, O. Wieland, M. Winkler and the RISING Collaboration, *Phys. Lett. B* **622**, 29 (2005).

[9] M. Honma, T. Otsuka, B.A. Brown and T. Mizusaki, *Phys. Rev. C* **65**, 061301(R) (2002).

[10] S.N. Liddick, P.F. Mantica, R.V.F. Janssens, R. Broda, B.A. Brown, M.P. Carpenter, B. Fornal, M. Honma, T. Mizusaki, A.C. Morton, W.F. Mueller, T. Otsuka, J. Pavan, A. Stolz, S.L. Tabor, B.E. Tomlin and M. Wiedeking, *Phys. Rev. Lett.* **92**, 072502 (2004).

[11] M. Honma, T. Otsuka, B.A. Brown and T. Mizusaki, *Eur. Phys. J. A* **25**, 499 (2005).

[12] V. Paar, *Nucl. Phys.* **A211**, 29 (1973).

[13] M.E. Bunker and J.W. Starner, *Phys. Rev.* **97**, 1272 (1955).

[14] P.F. Mantica, B.A. Brown, A.D. Davies, T. Glasmacher, D.E. Groh, M. Horoi, S.N. Liddick, D.J. Morrissey, A.C. Morton, W.F. Mueller, H. Schatz, A. Stolz and S.L. Tabor, *Phys. Rev. C* **68**, 044311 (2003).

[15] S. Zhu, R.V.F. Janssens, B. Fornal, S.J. Freeman, M. Honma, R. Broda, M.P. Carpenter, A.N. Deacon, B.P. Kay, F.G. Kondev, W. Królas, J. Kozemczak, A. Larabee, T. Lauritsen, S.N. Liddick, C.J. Lister, P.F. Mantica, T. Otsuka, T. Pawlat, A. Robinson, D. Seweryniak, J.F. Smith, D. Steppenbeck, B.E. Tomlin, J. Wrzesiński and X. Wang, *Phys. Lett. B* **650**, 135 (2007).

[16] J.G. Pronko, T.T. Bardin and J.A. Becker, *Phys. Rev. C* **13**, 608 (1976).

[17] S.N. Liddick, P.F. Mantica, R. Broda, B.A. Brown, M.P. Carpenter, A.D. Davies, B. Fornal, M. Horoi, R.V.F. Janssens, A.C. Morton, W.F. Mueller, J. Pavan, H. Schatz, A. Stolz, S.L. Tabor, B.E. Tomlin and M. Wiedeking, *Phys. Rev. C* **72**, 054321 (2005).

[18] S.N. Liddick, P.F. Mantica, R. Broda, B.A. Brown, M.P. Carpenter, A.D. Davies, B. Fornal, T. Glasmacher, D.E. Groh, M. Honma, M. Horoi, R.V.F. Janssens, T. Mizusaki, D.J. Morrissey, A.C. Morton, W.F. Mueller, T. Otsuka, J. Pavan, H. Schatz, A. Stolz, S.L. Tabor, B.E. Tomlin and M. Wiedeking, *Phys. Rev. C* **70**, 064303 (2004).

[19] B. Fornal, S. Zhu, R.V.F. Janssens, M. Honma, R. Broda, P.F. Mantica, B.A. Brown, M.P. Carpenter, P.J. Daly, S.J. Freeman, Z.W. Grabowski, N.J. Hammond, F.G. Kondev, W. Królas, T. Lauritsen, S.N. Liddick, C.J. Lister, E.F. Moore, T. Otsuka, T. Pawlat, D. Seweryniak, B.E. Tomlin and J. Wrzesiński, *Phys. Rev. C* **70**, 064304 (2004).

[20] D.J. Morrissey, B.M. Sherrill, M. Steiner, A. Stolz and I. Wiedenhöver, *Nucl. Instrum. Methods Phys. Res. B* **204**, 90 (2003).

[21] J.I. Prisciandaro, A.C. Morton and P.F. Mantica, *Nucl. Instrum. Methods Phys. Res. A* **505**, 140 (2003).

[22] P.F. Mantica, R. Broda, H.L. Crawford, A. Damaske, B. Fornal, A.A. Hecht, C. Hoffman, M. Horoi, N. Hoteling, R.V.F. Janssens, J. Pereira, J.S. Pinter, J.B. Stoker, S.L. Tabor, T. Sumikama, W.B. Walters, X. Wang and S. Zhu, *Phys. Rev. C* **77**, 014313 (2008).

[23] W.F. Mueller, J.A. Church, T. Glasmacher, D. Gutknecht, G. Hackman, P.G. Hansen, Z. Hu, K.L. Miller and P. Quirin, *Nucl. Instrum. Methods Phys. Res. A* **466**, 492 (2001).

[24] H.L. Crawford, R.V.F. Janssens, P.F. Mantica, J.S. Berryman, R. Broda, M.P. Carpenter, B. Fornal, G.F. Grinyer, N. Hoteling, B. Kay, T. Lauritsen, K. Minamisono, I. Stefanescu, J.B. Stoker, W.B. Walters and S. Zhu, *Acta Phys. Pol. B* **40**, 481 (2009).

[25] S. McDaniel, A. Gade, R.V.F. Janssens, D. Bazin, B.A. Brown, C.M. Campbell, M.P. Carpenter, J.M. Cook, A.N. Deacon, D.-C. Dinca, S.J. Freeman,

T. Glasmacher, P.G. Hansen, B.P. Kay, P.F. Mantica, W.F. Mueller, J.R. Terry, J.A. Tostevin and S. Zhu, Phys. Rev. C **81**, 024301 (2010).

[26] M. Langevin, C. Détraz, D. Guillemaud-Mueller, A.C. Mueller, C. Thibault, F. Touchard, G. Klotz, C. Miehé, G. Walter, M. Epherre and C. Richard-Serre, Phys. Lett. **130B**, 251 (1983).

[27] O. Sorlin, V. Borrel, S. Grévy, D. Guillemaud-Mueller, A.C. Mueller, F. Pougheon, W. Böhmer, K.-L. Kratz, T. Mehren, P. Möller, B. Pfeiffer, T. Rauscher, M.G. Saint-Laurent, R. Anne, M. Lewitowicz, A. Ostrowski, T. Dörfler and W.-D. Schmidt-Ott, Nucl. Phys. A **632**, 205 (1998).

[28] L.A. Parks, C.N. Davids and R.C. Pardom, Phys. Rev. C **15**, 730 (1977).

[29] B. Fornal, S. Zhu, R.V.F. Janssens, M. Honma, R. Broda, B.A. Brown, M.P. Carpenter, S.J. Freeman, N. Hammond, F.G. Kondev, W. Królas, T. Lauritsen, S.N. Liddick, C.J. Lister, S. Lunardi, P.F. Mantica, N. Marginean, T. Mizusaki, E.F. Moore, T. Otsuka, T. Pawlat, D. Seweryniak, B.E. Tomlin, C.A. Ur, I. Wiedenhöver and J. Wrzesiński, Phys. Rev. C **72**, 044315 (2005).

[30] N. Cieplicka *et al.*, in preparation.

[31] G. Audi, A.H. Wapstra and C. Thibault, Nucl. Phys. A **729**, 337 (2003).

[32] T. Dörfler, W.-D. Schmidt-Ott, T. Hild, T. Mehren, W. Böhmer, P. Möller, B. Pfeiffer, T. Rauscher, K.-L. Kratz, O. Sorlin, V. Borrel, S. Grévy, D. Guillemaud-Mueller, A.C. Mueller, F. Pougheon, R. Anne, M. Lewitowicz, A. Ostrowsky, M. Robinson and M.G. Saint-Laurent, Phys. Rev. C **54**, 2894 (1996).

[33] R. Grzywacz, R. Béraud, C. Borcea, A. Emsalem, M. Głogowski, H. Grawe, D. Guillemaud-Mueller, M. Hjorth-Jensen, M. Houry, M. Lewitowicz, A.C. Mueller, A. Nowak, A. Płochocki, M. Pfützner, K. Rykaczewski, M.G. Saint-Laurent, J.E. Sauvestre, M. Schaefer, O. Sorlin, J. Szerypo, W. Trinder, S. Viteritti and J. Winfield, Phys. Rev. Lett. **81**, 766 (1998).

[34] P. Maierbeck, R. Gernhäuser, R. Krücken, T. Kröll, H. Alvarez-Pol, F. Aksouh, T. Aumann, K. Behr, E.A. Benjamim, J. Benlliure, V. Bildstein, M. Böhmer, K. Boretzky, M.J.G. Borge, A. Brünle, A. Bürger, M. Caamaño, E. Casarejos, A. Chatillon, L.V. Chulkov, D. Cortina-Gil, J. Enders, K. Eppinger, T. Faestermann, J. Friese, L. Fabbietti, M. Gascón, H. Geissel, J. Gerl, M. Gorska, P.G. Hansen, B. Jonson, R. Kanungo, O. Kiselev, I. Kojouharov, A. Klimkiewicz, T. Kurtukian, N. Kurz, K. Larsson, T. Le Bleis, K. Mahata, L. Maier, T. Nilsson, C. Nociforo, G. Nyman, C. Pascual-Izarra, A. Perea, D. Perez, A. Prochazka, C. Rodriguez-Tajes, D. Rossi, H. Schaffner, G. Schrieder, S. Schwertel, H. Simon, B. Sitar, M. Stanoiu, K. Sümmerer, O. Tengblad, H. Weick, S. Winkler, B.A. Brown, T. Otsuka, J. Tostevin and W.D.M. Rae, Phys. Lett. B **675**, 22 (2009).

[35] P.F. Mantica, A.C. Morton, B.A. Brown, A.D. Davies, T. Glasmacher, D.E. Groh, S.N. Liddick, D.J. Morrissey, W.F. Mueller, H. Schatz, A. Stoltz, S.L. Tabor, M. Honma, M. Horoi and T. Otsuka, Phys. Rev. C **67**, 014311 (2003).

[36] O. Sorlin, C. Donzaud, F. Azaiez, C. Bourgeois, L. Gaudemard, F. Ibrahim, D. Guillemaud-Mueller, F. Pougheon, M. Lewitowicz, F. de Oliveira Santos, M.G. Saint-Laurent, M. Stanoiu, S.M. Lukyanov, Yu.E. Penionzhkevich, J.C. Angélique, S. Grévy, K.-L. Kratz, B. Pfeiffer, F. Nowacki, Z. Dlouhy and J. Mrasek, Nucl. Phys. A **719**, 193c (2003).

[37] S. Bhattacharyya, M. Rejmund, A. Navin, E. Caurier, F. Nowacki, A. Poves, R. Chapman, D. O'Donnell, M. Gelin, A. Hodsdon, X. Liang, W. Mittig, G. Mukherjee, F. Rejmund, M. Rousseau, P. Roussel-Chomaz, K.-M. Spohr and Ch. Theisen, Phys. Rev. C **79**, 014313 (2009).

[38] D.E. Alburger, E.K. Warburton and B.A. Brown, Phys. Rev. C **30**, 1005 (1984).

[39] U. Fister, R. Jahn, P. von Neumann-Cosel, P. Schenk, T.K. Trelle, D. Wenzel and U. Wienands, Nucl. Phys. A **569**, 421 (1994).

[40] F. Ajzenberg-Selove, R.E. Brown, E.R. Flynn and J.W. Sunier, Phys. Rev. C **32**, 756 (1985).

[41] V. Paar, Nucl. Phys. A **331**, 16 (1979).

[42] A. Gade, R.V.F. Janssens, D. Bazin, B.A. Brown, C.M. Campbell, M.P. Carpenter, J.M. Cook, A.N. Deacon, D.-C. Dinca, S.J. Freeman, T. Glasmacher, B.P. Kay, P.F. Mantica, W.F. Mueller, J.R. Terry and S. Zhu, Phys. Rev. C **73**, 037309 (2006).

[43] B. Fornal, R.V.F. Janssens, R. Broda, N. Marginean, S. Beghini, L. Corradi, M.P. Carpenter, G. De Angelis, F. Della Vedova, E. Farnea, E. Fioretto, A. Gadea, B. Guiot, M. Honma, W. Królas, T. Lauritsen, S. Lunardi, P.F. Mantica, P. Mason, G. Montagnoli, D.R. Napoli, T. Otsuka, T. Pawlat, G. Pollaro, F. Scarlascara, A.M. Stefanini, D. Seweryniak, S. Szilner, C.A. Ur, M. Trotta, J.J. Valiente-Dobón, J. Wrzesiński and S. Zhu, Phys. Rev. C **77**, 014304 (2008).

[44] S.P. Pandya, Phys. Rev. **103**, 956 (1956).

[45] A. Poves, J. Sánchez-Solano, E. Caurier, and F. Nowacki, Nucl. Phys. A, **694**:157, 2001.